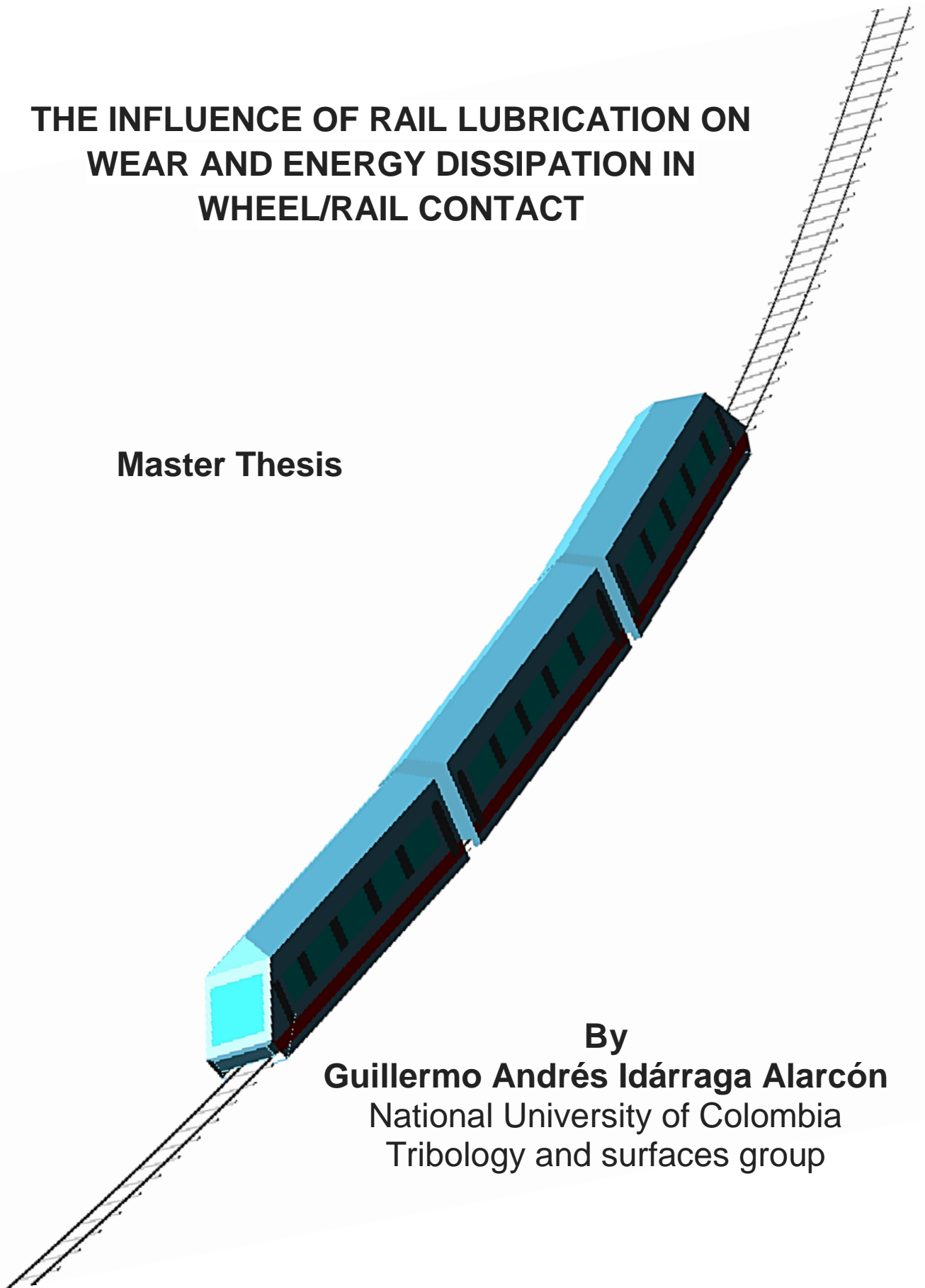


THE INFLUENCE OF RAIL LUBRICATION ON WEAR AND ENERGY DISSIPATION IN WHEEL/RAIL CONTACT

Master Thesis



By
Guillermo Andrés Idárraga Alarcón
National University of Colombia
Tribology and surfaces group



THE INFLUENCE OF RAIL LUBRICATION ON WEAR AND ENERGY DISSIPATION IN WHEEL/RAIL CONTACT

GUILLELMO ANDRÉS IDÁRRAGA ALARCÓN
MECHANICAL ENGINEER



NATIONAL UNIVERSITY OF COLOMBIA
FACULTY OF MINES
SCHOOL OF MINERALS AND MATERIALS
MEDELLÍN
2015



THE INFLUENCE OF RAIL LUBRICATION ON WEAR AND ENERGY DISSIPATION IN WHEEL/RAIL CONTACT

Academic thesis, which with the approval of the National University of Colombia, will be presented for public review in fulfillment of the requirements for a Degree of Master.

Eng. Guillermo Andrés Idárraga Alarcón

National University of Colombia.

Tribology and Surfaces Group

gaidarra@unal.edu.co

ADVISOR:

Alejandro Toro Betancur Ph.D.

National University of Colombia.

Tribology and Surfaces Group

aotoro@unal.edu.co

CO-ADVISOR:

Juan Manuel Meza Meza Ph.D.

National University of Colombia.

Tribology and Surfaces Group

jmmezam@unal.edu.co

INTERNATIONAL ADVISOR:

M.Sc. Nico Burgelman

Delft University of Technology

Department of Railway Engineering

+31 (0) 643963939

N.D.M.Burgelman@tudelft.nl



**I dedicate this dissertation to
my mother Consuelo, my sister Katherine
and my lovely Magaly**

“Not everything that’s cool is science, but everything in science is cool”
Phil Plait.



ACKNOWLEDGMENTS

The research presented in this thesis was supported by Joven Investigador of Colciencias scholarship, Enlaza Mundos of Medellin municipality scholarship, Tribology and Surfaces Group (GTS) at the National University of Colombia, and the Railway Engineering Group at Delft University of Technology (TU Delft).

Doing a master and finalizing it with a thesis is an excruciating task that cannot be done without the help and support of many special people. I would therefore like to start by thanking Professor Alejandro Toro Betancur for giving me the opportunity to do this project at an esteemed institution such as the National University of Colombia. He always trusts me with my job. I am very grateful for his advice and guidance. I owe deep gratitude to Professor Juan Meza, head of GTS, who allowed me to be part of the Joven Investigador of Colciencias scholarship, improve my research skills, and complete my research on-time. I would also like to thank Juan Felipe Santa for all his help and advice during my research period and for giving me the freedom to explore my ideas.

My gratitude goes as well to professor Zili Li, who gave me the opportunity to come to Delft and guided me through all the stages of my internship at the Railway Engineering Group at TU Delft. I am also grateful to Professor Rolf Dollevoet for his cooperation during my research project.

I would particularly acknowledge Nico Burgelman for his clear explanation, feedback, and problem analysis, which helped me a lot during my research at TU Delft. I highly appreciate that you never lost your helpful attitude and you always were willing to share your knowledge with me.

I also would like to express my appreciation to all the members of the Railway Engineering Group, especially Dr. Alfredo Nuñez for his guidance during my stay in Delft. I also should not forget my officemate Pungky and her husband Senot, who made my work at TU Delft pleasant.

I owe my gratitude to the secretary of Railway Engineering Group at TU Delft, Jacqueline Barnhoorn. Thank you very much for all your help in navigating through bureaucracy and administrative procedures.

A special word goes to Yuliana; it was great to have you as a colleague, thanks for your suggestion, explanation and especially for your friendship. A special “thank you” also goes to the GTS group colleagues: Andrey, Alejandro, Paula, Camilo, Santiago, Sergio, Diego, Jaime, and Jesus. I acknowledge you all!



I am also very happy that I have had the opportunity to collaborate with industry and to see my know-how applied in the “real world”. For this I thank Mauricio Palacio and Rodrigo Toro from the Metro of Medellín who gave me the opportunity to work for an excellent company as the Metro of Medellín, thank you for your suggestions, data and personal recommendations. Special thanks also go to the Metro of Medellín technician Miguel Angel Fernandez, thanks for your availability and willingness to help me during the track visits.

During my Master’s studies, I got to know great friends who helped me reset my mind when I needed it the most. Daniel in Colombia and Khaled in The Netherlands are my best friends, the meaning of “parce” would not have sense without you.

Now it is time for special words to the people closest to my heart. To my mother Consuelo and my sister Katherine: thank you for encouraging me to follow my studies and supporting me through all these years. To Magaly: my love, you always understood when I had to work instead of spending time together. To Cielo: thank you for your love and inspiration. To them I dedicate this thesis, without your support I would have never reached this far.



ABSTRACT

This work investigates the energy dissipation in a wheel/rail system with field measurements and friction work modelling. Friction and contact conditions are measured and analyzed in order to calculate the power saving of one vehicle running over a curve of a metro line. For modelling the contact forces, creepages and spin between the wheels and rails are determined via simulations of a train travelling in a curve of the track. Next the contact stress and the micro-slip in the contact area are computed from the forces, creepages and spin as well as the measured friction coefficient and profiles of wheels and rail. Three friction conditions are tested: dry, lubricated with a friction modifier and a post lubricated condition. The total frictional work is obtained by integrating local frictional dissipation over the contact area. The wear is also analyzed according to the Ty method including the spin, in combination with Kalker's simplified theory, assuming that the wear is proportional to the frictional work. The frictional work is then related to the energy consumptions under the different friction conditions, which allows evaluating the effectiveness of the friction modifier and its influence on the wear of the wheel/rail system.

Keywords: Multi-body simulation; Frictional work; Energy consumption; Lubricants; Wheel/rail wear.



RESUMEN

Este trabajo investiga la disipación de energía en un sistema rueda/riel a través de mediciones de campo y modelación de trabajo de fricción. Las condiciones de fricción y de contacto son medidas y analizadas con el fin de calcular el ahorro de potencia de un vehículo ferroviario sobre una curva de una línea metro. Para la modelación, las fuerzas de contacto, tasas de deslizamiento y giro entre las ruedas y los rieles, son determinados a través de simulaciones de un tren viajando en una curva específica de la vía. Posterior a esto, los esfuerzos de contacto y el micro-deslizamiento son calculados por medio de las fuerzas, tasas de deslizamiento y giro, así como las mediciones de coeficiente de fricción y perfiles de las ruedas y rieles. Tres condiciones de fricción son estudiadas: seco, lubricado con un modificado de fricción y una condición post-lubricante. El trabajo total por fricción es obtenido integrando la disipación local sobre el área de contacto. El desgaste es también analizado utilizando el método Ty incluyendo el giro, en combinación con la teoría simplificada de Kalker, asumiendo que el desgaste es proporcional al trabajo de fricción. El trabajo de fricción es por lo tanto, relacionado con los consumos de energía bajo las diferentes condiciones de fricción, lo cual permite evaluar la efectividad de los modificadores de fricción y su influencia en el desgaste del sistema rueda/riel.

Palabras Claves: Simulación Multicuerpo, Trabajo por Fricción, Consumo de Energía, Lubricantes, Desgaste Rueda/Riel.



TABLE OF CONTENTS

	CHAPTER 1
INTRODUCTION	
1.1 Introduction.....	1
	CHAPTER 2
PROBLEM STATEMENT	
2.1 Problem statement.....	2
	CHAPTER 3
LITERATURE REVIEW	
3.1 Wear of wheel/rail systems.....	8
3.1.1 Wheels wear.....	8
3.1.1.1 Adhesion.....	9
3.1.1.2 Corrosive wear.....	10
3.1.1.3 Wheel rolling contact fatigue	10
3.1.1.4 Plastic deformation.....	11
3.1.2 Rail wear.....	12
3.1.2.1 Rail rolling contact fatigue.....	13
3.1.2.2 Rail corrugation.....	14
3.1.3 Wear regimes.....	14
3.1.4 Wear transitions.....	17
3.1.5 Wear modeling.....	19
3.2 Wheel – rail contact.....	20
3.2.1 Traction coefficient.....	23
3.3 Railway vehicles.....	24
3.3.1 Bogies.....	24
3.3.1.1 Tilting bogie.....	26
3.3.1.2 Steering bogie.....	26
3.3.2 Bogie frame.....	27
3.3.2.1 Rigid frame Bogie.....	27
3.3.2.2 Three-Piece bogie frame.....	27
3.3.3 Suspension elements.....	28
3.3.3.1 Primary suspension.....	28
3.3.3.1.1 Axle box suspension.....	28
3.3.3.2 Secondary Suspension.....	30
3.4 Computer simulation.....	31
3.4.1 Multibody simulation (MBS).....	31
3.4.2 Wear modeling using multibody simulation.....	32
3.5 Friction modifiers and lubrication system.....	34
3.5.1 Friction modifiers.....	34
3.5.2 Lubrication Systems.....	36
3.5.2.1 Lubricants delivery systems on-board.....	36
3.5.2.2 Stationary rail lubrication systems.....	36



CHAPTER 4

OBJECTIVES

4.1 General Objective.....	37
4.2 Specific Objectives.....	37

CHAPTER 5

METHODOLOGY

5.1 Lubrication system selection and installation.....	38
5.1.1 Selection of the lubrication system.....	38
5.1.1.1 Hy-Power system description.....	40
5.1.2 Installation of the lubrication system.....	41
5.2 Friction coefficient measurements.....	42
5.3 Energy measurements.....	43
5.4 Multibody model development.....	44
5.4.1 The vehicle model.....	44
5.4.2 The track model.....	48
5.5 Energy and wear calculations.....	49
5.5.1 The wheel/rail contact problem.....	49
5.5.2 Energy calculations.....	49
5.5.3 Wear calculations.....	50

CHAPTER 6

RESULTS AND DISCUSION

6.1 Friction coefficient measurement in the field.....	51
6.2 Power consumption measurement in the field	52
6.3 Calculation of the moment of force of a Wheel	55
6.4 Power and wear calculations.....	57
6.4.1 Power calculations.....	57
6.4.2 Wear calculations.....	65
6.4.3 Profiles effect in the energy consumption and wear rates.....	67

CHAPTER 7

CONCLUSIONS AND RECOMMENDATIONS

7.1 Conclusions and recommendations.....	71
--	----

REFERENCES	73
-------------------	-----------

**INTRODUCTION**

Lubricants have been widely used in railway systems in order to increase the lifetime of the wheel and rail, as well as to decrease the maintenance and operating expenses. There are two types of lubrication systems: stationary systems, which are installed along the tracks, and on-board systems, which move with a train and where the lubricants are often applied to the flanges of the wheels. Lubrication has traditionally been employed to reduce friction and wear. Currently, at the top of the rails a special type of lubricants is applied to ensure a stable coefficient of friction, which is required in operations such as accelerating and braking. These kinds of lubricants are called friction modifiers (FM). FM's are lubricant greases with a high content of abrasive particles which produce micro abrasion in the contact, keeping the friction coefficient at a target value for the system [1]. According to [2], an appropriate value of the friction coefficient is 0.35, but this optimum value depends on the characteristics of the systems, such as, the velocity, axle load and the radius of the curve.

Implementing effective lubrication strategies on small radius curves allows for a reduction of the wheel's wear, the rail's wear and the noise level. A research carried out in the UK by the Engineering Research Program in 2003 [3], shows that by using lubricants the rail life span can be increased by a factor two, the wheel life span by a factor five and the re-profiling intervals of the wheel and rail can be also extended by a factor four.

As mentioned above, it is possible to reduce the operation costs through the implementation of lubrication systems. According to Reddya et al. [4], a 12 MGT transportation system can save around 2.4% for 0–300 m curves, 9.1% for 300–450 m curves and 15.5% for 450–600 m curves of operation cost, by proper planning of the intervals for rail grinding and using an adequate lubrication for its interface.

For the Metro of Medellín the energy-related operation costs reached US\$ 9.34 million per year of which US\$ 6.74 million is related to the traction of the vehicles. The study of the energy consumption associated with the contact between the wheel and the rail is a first step towards understanding the mechanisms that deteriorate these components. This understanding will allow further reductions of the operation costs.

To such an end, this work examines the effect of three contact conditions: dry, lubricated with a commercial friction modifier and a post lubricated condition, on the energy consumption and wear rates of the system at a specific section of the Metro of Medellín. The approach consists of two mutually interactive parts: field measurements of the energy consumption of the vehicle and the friction coefficient, and simulations of the energy dissipated in the wheel/rail contact interface using multi-body simulation and the Ty method [5], including the contribution of the spin based on Kalker's simplified theory [6, 7].



CHAPTER 2

PROBLEM STATEMENT

The Metro of Medellín Company is an integral transportation system with three cable lines, two commercial and one dedicated to the tourism, three buses lines and two railway lines. The Metro of Medellín has planned increase its service with one tram line and two cable lines by 2016, see the Figure 1a.

Its railway lines measure 30.9 Km. Line A is 25.3 km long with twenty one stations and Line B has 5.6 km with six stations (the blue and orange lines respectively in the Figure 1b). For this work the section of interest is the curve 4, located between the stations San Javier and Santa Lucía on line B, where a stationary lubrication system is installed.

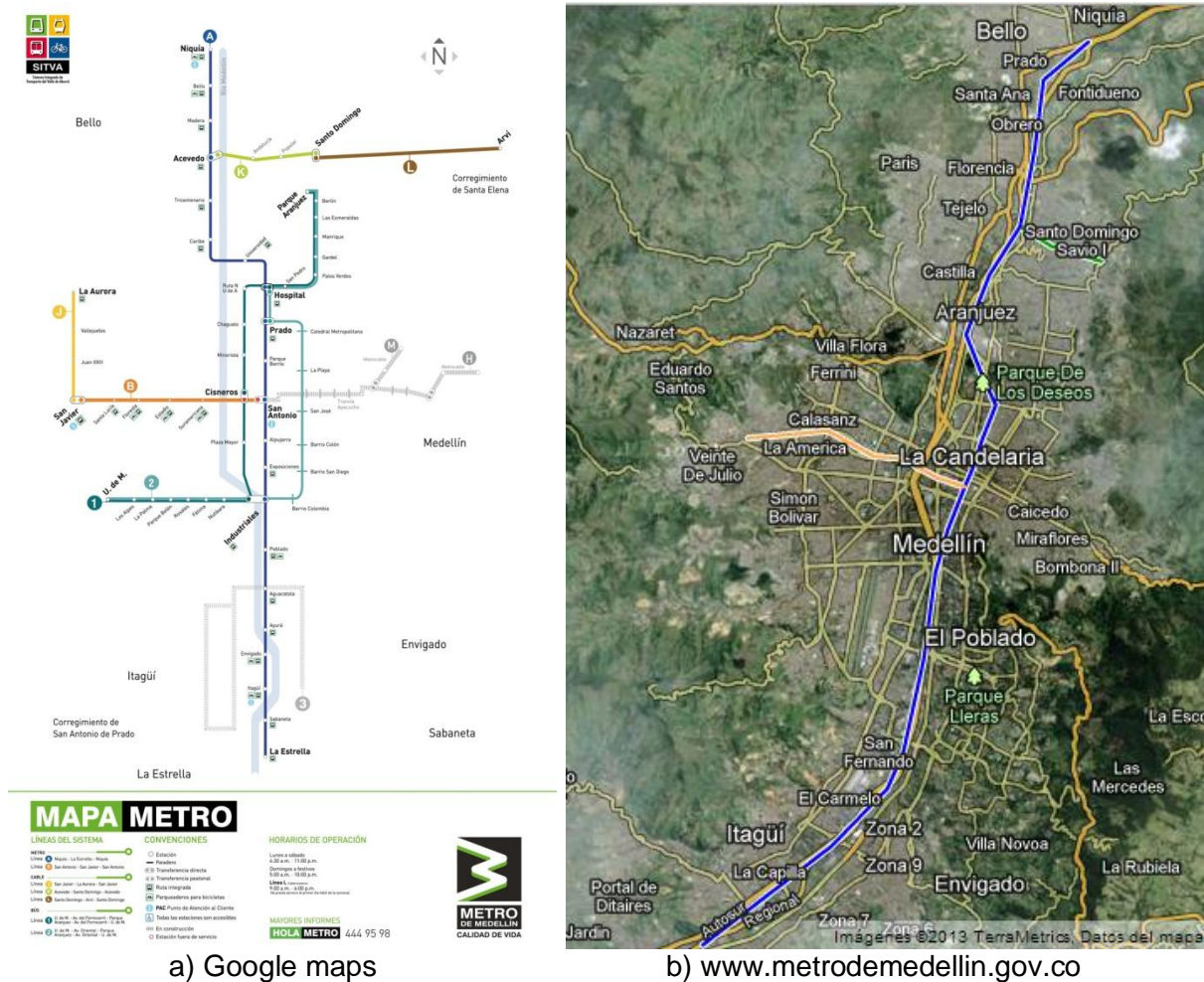


Figure 1. Metro of Medellín map. a) Scheme of the Medellín transportation system, b) Satellite view of railway lines.



In order to identify the main defects in rails of the Metro of Medellín, several track visits were performed in all the curves of the line B over a two year period. Figure 2a to 2f show the most important defects found in the commercial line [8]. The main defects are rolling contact fatigue (RCF), particularly head checks and spalling, and corrugation. The latter is mostly visible at the contact patch in sharp curves.



Figure 2. Common defects of the Metro of Medellín tracks. a) Adhesion, b) Class A – light Squat, c) Head checks, d) Spalling, e) Rolling contact Fatigue, f) Plastic flow.



Corrugation was first defect detected on the Metro of Medellín tracks several years ago. The problem was controlled by replacing the rails and wheels profiles as a result of an optimization analysis performed by the National Research Council NRC [9] and reducing the mean time between re-profiling of the rails in some sharp curves. Despite these measures, corrugation is still present in several critical points of the railway

In order to control the defects on the rails, re-profiling procedures are executed at a frequency of once every 3 months for the worst curve and around 5-7 months for other curves [10]. A research carried out by P.A. Cuervo et al. [11] shows the percentage of the total grinding operation for the high and low rail in the line B of the Metro of Medellín. The defects that triggered the grinding operation are shown in Figure 3: fatigue, corrugation and large deviation from the nominal rail profile. It can be concluded that fatigue marks are mainly an issue for the high rail, whereas corrugation and loss of profile by wear are the most important defects found on the low rail. Note most of the grinding operations (58%) are caused by defects on the high rail.

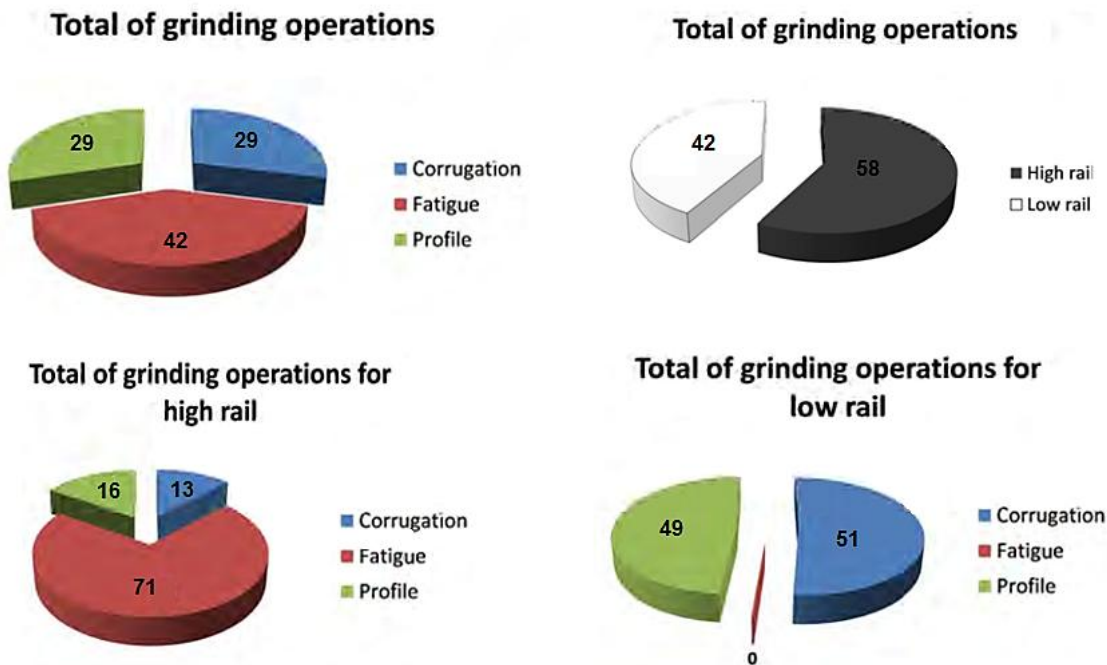


Figure 3. Details of grinding operations performed in the field [11].

J.F Santa [1] calculated the wear rate and identified most important causes of damage in all curves of the Metro of Medellín line B over a period of 9 years. To such an end historical data (including Miniprof measurements) was processed, analyzed and related to some specific operation conditions and maintenance tasks. The wear rates were calculated as the mean slope of a straight line fitted to the data resulting from the cumulated traffic as a function of the material loss from the head of the rail for each curve. For the material loss,



the vertical wear ($W1$) was used since it is the criterion used in the field to determine whether a rail must be changed, see Figure 4.

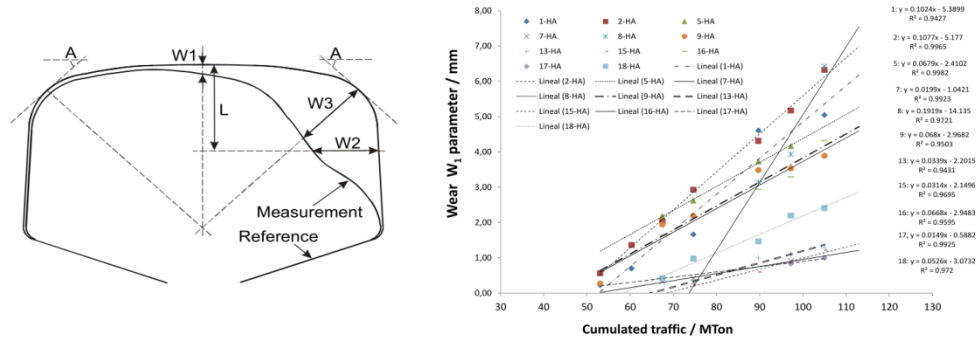


Figure 4. Detail of material losses because of rolling sliding wear and grinding in a curve of Metro de Medellín [1].

The first interesting conclusion is that most of the curves fitted a straight line very well and this behavior is unexpected, bearing in mind that the data is collected from the field. Which means that the grinding operators use the same grinding depth, not taking into account the actual depth of the defects.

Figure 5 shows the wear rates (WR) calculated by J.F Santa for the line B, they were classified as mild, medium and high, depending on the magnitude of the wear rate (WR). The mild wear regime corresponds to $WR < 0.06$ mm/MTon, the medium wear regime is defined as 0.06 mm/MTon $< WR < 0.2$ mm/MTon while the severe wear regime occurs for $WR > 0.2$ mm/MTon. According to the results the wear rates are two (2) to six (6) times higher than those found in the literature for metros. The WR 's in the metro of Medellín are similar to those observed in heavy haul lines [12]. Moreover, when the wear rates of high and low rails are compared, the high rail is two times higher than the low rail.

To improve the performance of the Metro of Medellín tracks, a lubrication strategy was implemented. The results of the wear rates were a starting point to identify the most strategic location to install the commercial lubrication system used for this work. The curve 4 was selected because it has a high wear rate and there is enough space in the field side to perform the maintenance and review procedures.



WEAR RATE OF RAILS / mmMTon⁻¹

Curve number	18	17	16	15	14	9	8	7	5	2	1
Wear rate of high rail	0.05	0.01	0.07	0.03	0.17	0.07	0.19	0.02	0.07	0.11	0.10
Wear rate of Low rail	0.03	-	0.04	0.05	-	0.05	0.11	0.03	0.04	0.07	-

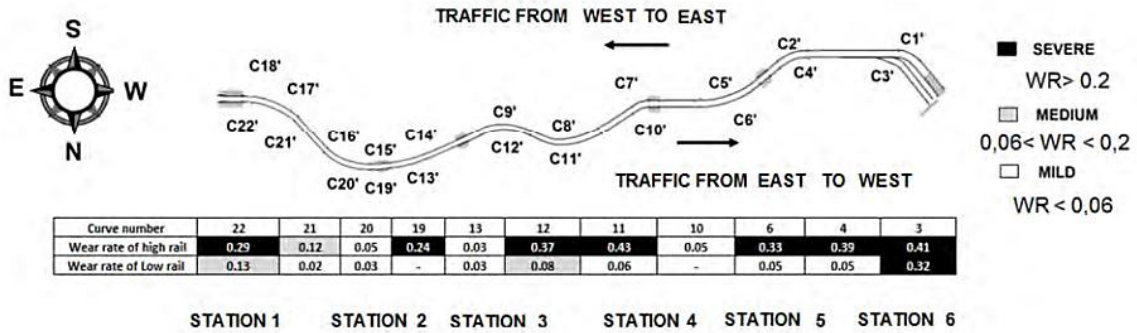


Figure 5. Wear rates of the curves of the entire line [1].

J.F Santa also compared the wear caused by grinding (artificial wear) and the wear by rolling sliding, where the latter could be abrasive wear, adhesive wear and wear from tribochemical reactions. The results show that the grinding wear is larger compared with rolling sliding, as a matter of fact, the artificial wear is be 5 times higher. Metallographic inspection of the rails after performing grinding procedures revealed a hard white layer with cracks parallel to the surface [13]. This layer is composed of fresh martensite formed due to localized heating and fast cooling during the grinding, which indicates that maintenance operations can be responsible for additional problems. These results together with the short re-profiling period, explains the high wear rates present in the Metro of Medellín.

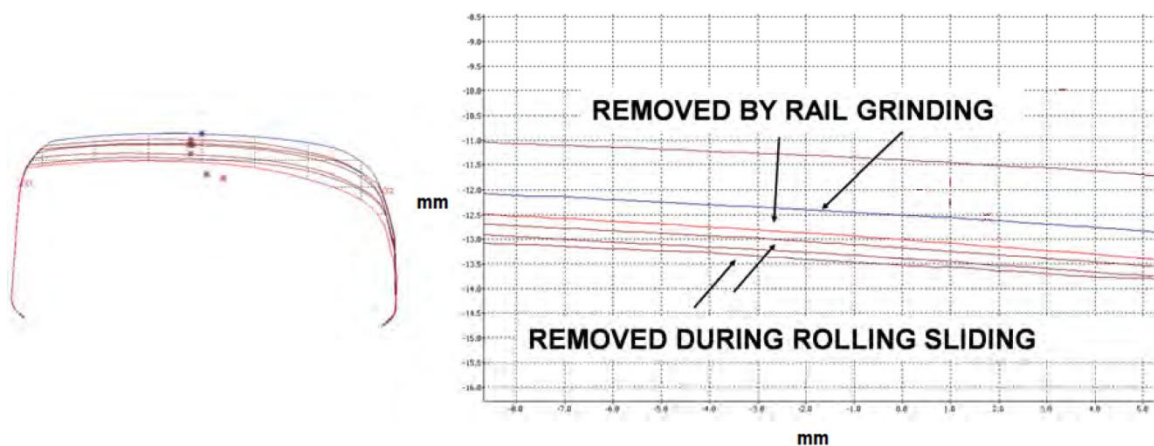


Figure 6. Detail of material losses due to rolling sliding wear and grinding in a curve of the Metro de Medellín [1].



The implementation of friction modifiers in combination with proper grinding procedures has emerged as a solution to improve the efficiency and decrease the wear rates of the system. However, a further understanding of the influence of the rail lubrication on wear and energy dissipation in the wheel/rail contact is necessary. Wheel/rail contact simulations using multibody analysis allows the prediction of the behavior of the friction modifiers (friction coefficient) in an economical and efficient way. This type of analysis has not been done in the Metro of Medellín and there is a lack of fundamental knowledge related to the performance of the wheel/rail interface with an energy approach.

**LITERATURE REVIEW**

3.1 Wear of wheel/rail systems

The wear on the wheel-rail interface is one of the most critical problems in railway systems, due to the high maintenance costs that it generates, which could reach to U.S \$ 54 total annual per meter and U.S. \$ 1.5 million for a 30 km route [3]. The profiles of the wheels and rails change significantly due to wear, changing the wheel-rail contact geometry, increasing vehicle-track dynamic forces and reducing the performance and dynamics characteristics of the vehicles such as the stability or passenger comfort.

The wear of wheel/rail systems can be divided in wear of rails and wear of wheels. Wear of the wheels is controlled by re-profiling, which is performed each 80000 km in the case of the Metro of Medellín. However this procedure is limited by the mechanical resistance of the wheel. When this limit is reached, the wheel has to be replaced. On the other hand, the wear of the rail can be divided in wear of the gauge corner and wear of the top of the rail. In sharp curves, the wear of the gauge is dominant. In straight lines, the wear of the top of the rails is more significant. However, in both regions, the most important mechanism is fatigue due to the high loads transmitted along the wheel-rail interface.

3.1.1 Wheels wear

The life of railway wheels is usually limited by wear. The wheel surface is subjected to high normal and tangential contact stress. Contact forces change their magnitude and orientation when the wheel travels over the rail curves, crossings, and local surface perturbations. The contact is mostly rolling but a small amount of local sliding takes place at the interface. The amount of sliding depends on the contact patch geometry, normal force, lateral force, and friction coefficient. The removal of material from the surface by wear is a function of the sliding and contact stresses [14].

Two main manifestations of wear typically occur on railway wheels: a change in the transversal profile, called 'regular wear', and the formation of periodic wear patterns in circumferential direction, called wheel out-of-roundness or 'irregular wear' [15]. Regular wear is produced by slow variations of contact forces and creepages associated with the longitudinal and lateral motion of the wheelset on the track, on straight lines and in curves. On the other hand, irregular wear is produced by fast variations of wheel-rail contact conditions, which are produced by train-track interaction and are strongly affected by the vertical vibrations of the system.

In traction and braking, wear is produced by longitudinal tractive/braking efforts and tends to concentrate on the central portion of the wheel tread, while during curve negotiation the



wear process is more complicated, and it involves both longitudinal frictional forces caused by the rolling radius difference between the inner and outer wheels and transversal frictional forces caused by the yaw angle of the wheelset [16, 17]. As a consequence of this complex wheel-rail contact condition, two distinct wear regions appear on the wheel profile: one on the flange and the other the tread, see Figure 7. Wear rates in these two regions depend on different factors, such as the vehicle design, the service profile, the status of the contacting surfaces (including the possible presence of natural or artificial lubrication) and the mechanical properties of wheel and rail materials.

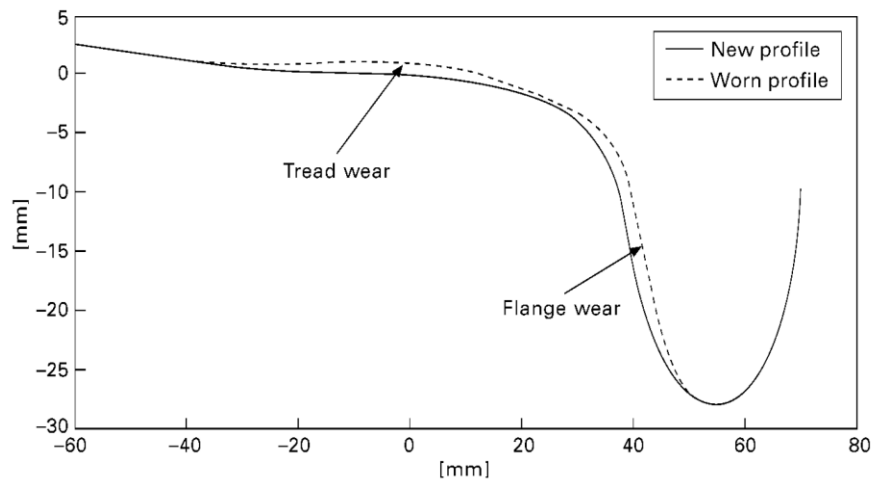


Figure 7. Wear regions on the wheel profile. [18]

The defects on a wheel are:

- Adhesive wear
- Corrosive wear
- Rolling contact fatigue (RCF)
- Plastic deformation

These four defects are further discussed in the following sections.

3.1.1.1 Adhesion

Under sliding conditions, typically during the acceleration, there is a high probability that the contact is broken and a small volume of material is torn off usually from the wheels (the softer material) and adhered to the top of rail. Figure 8 shows a typical burn mark on the rail, which is generated when the wheel loses adhesion and high slide rates take place.



Figure 8. Burn mark on the top of the rail by adhesion loss.

3.1.1.2 Corrosive wear

Corrosive wear is the result of the repetitive material removal produced by the chemical corrosion when a sliding action is performed. In rails, this type of wear is insignificant compared with wear produced by fatigue.

3.1.1.3 Wheel rolling contact fatigue

In classic fatigue analysis of components subjected to alternating stresses, the fatigue life is often related to the stress amplitude. Graphically this relation can be plotted in a stress-number (S-N) curve, also referred to as a Wohler curve, as outlined in Figure 9, in which at higher loads the fatigue life decreases exponentially with the stress magnitude. Regarding to railway wheels one wheel revolution will correspond to one load cycle.

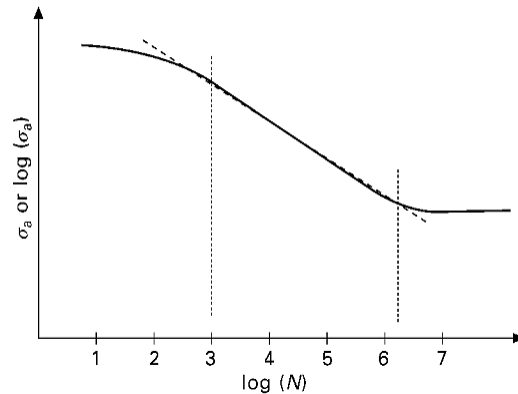


Figure 9. The Wohler (S-N) curve, where N is the number of load cycles and S is the logarithm of the stress [19].

In a loaded railway wheel, the contact stress field is multiaxial and has six independent components in each material point. To characterize the fatigue impact an equivalent scalar stress measure (similar to the use of von Mises or Tresca effective stresses in plasticity analysis) is employed. In principle, the derived equivalent stress could be introduced in a Wohler curve to give the resulting fatigue life [19]. In addition, the overall loading is essentially compressive. This will increase the resulting fatigue life, but to what extent depends on the load configuration.

Under RCF the wheel is submitted to slip and rolling. This condition allows that the contact stress zone moves along with the rolling component and therefore it is possible for initiated cracks to grow/extend to a significant length. Depending on the characteristics of the loading and the material resistance, RCF cracks may initiate at or below the surface.

3.1.1.4 Plastic deformation

Plastic deformation is caused by the high stresses on the contact, which take place either at the surface or subsurface depending of the friction coefficient. Figure 10 shows a shakedown map, which illustrates the relationship between friction in the wheel-rail contact and the load-carrying capacity of the contact. It shows the limits of material in terms of non-dimensional contact pressure, p_0/k as a function of friction coefficient, $\mu = T/N$, where p_0 is the normal contact pressure, k is the shear yield strength, T is the tractive force and N is the normal load. At relatively low friction coefficients, cumulative plastic flow occurs subsurface but for friction coefficients above about 0.3, the plastic flow is greatest on the surface. The worst position in terms of damage is in the ratcheting region, where the strain is accumulated until the ductility of the material is exceeded and it is torn off as wear debris or a surface crack is initiated [20, 21].

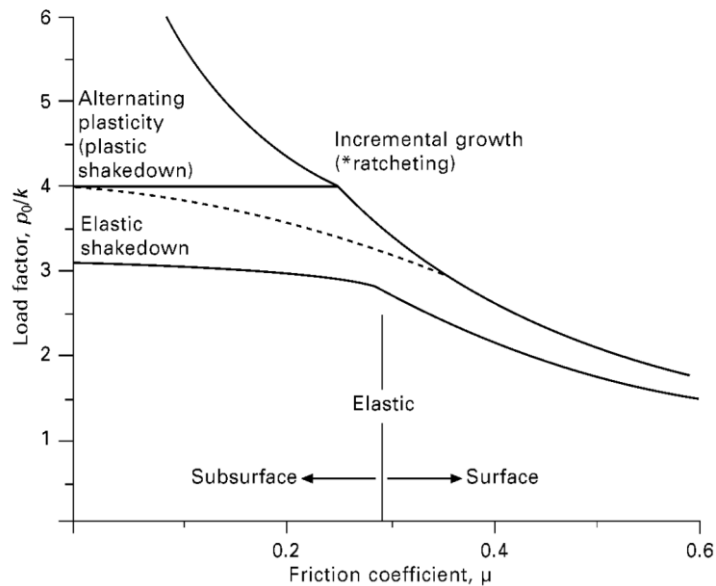


Figure 10. Shakedown map [20].

3.1.2 Rail wear

In recent years railways have experienced significant changes in the vehicle-track interaction, caused by an increase in axle load and operational speed. As consequence of these changes, higher stresses are produced at the wheel-rail interface. The situation is aggravated by track irregularities.

Track irregularities associated with low frequency vibration may cause discomfort to passengers and damage to cargo. Such irregularities, which normally have a length longer than 3 meters are often called long track irregularities. Examples of long track irregularities include poor track alignments, switches, level crossings and bridges.

Track irregularities shorter than about 3 meters are often referred to as short track irregularities. Examples of short track irregularities include squats, corrugation, thermite welds with poor finishing quality, insulated joints, blades and frogs of switches and crossings. They can cause large dynamic contact forces and wheel-rail vibrations in the mid and high frequency ranges. According to [21] the mid-frequency range is 40-400Hz and the high frequency is 400-2000Hz or even higher.

As previously mentioned, the most common failure mechanisms in the tracks of the Metro of Medellín are rolling contact fatigue and corrugation, therefore these topics will be the central focus of this section.

3.1.2.1 Rail rolling contact fatigue

There are several types of defects caused by fatigue:

- **Head checks** are initially small and micro-cracks on the rail surface, which grow down into the rail at an angle below the surface, as it is shown in Figure 11. As they enlarge, they may branch down causing a rail fracture, or branch up leading to spalling of the rail surface, see Figure 2d. This type of cracking is typically found on the high rail in the sharp curves.



Figure 11. Rail fatigue damage: a) head checks, b) depth and crack angle with respect to the rail surface.

- **Squats** are generally considered as surface initiated defects. Squats can be classified as being light, moderate and severe, or class A, B and C correspondingly see Figure 12. Light squats are also called early squats, initiating squats or squats seeds [22].

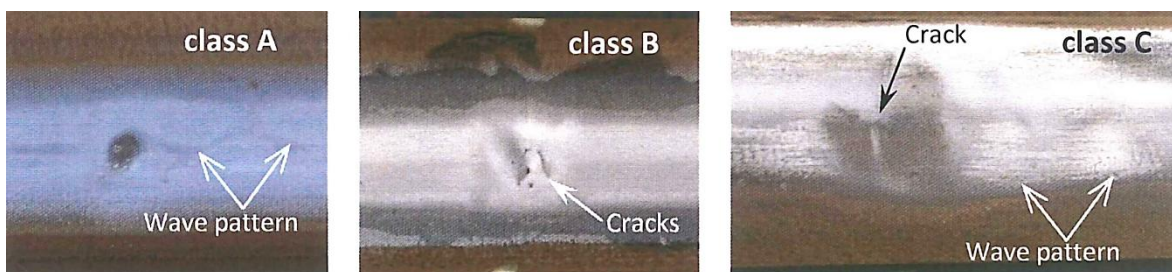


Figure 12. Squats: class A – light, class B – moderate and class C – severe [21].

A severe squat is normally characterized by localized depression of the contact surface of the rail head, accompanied by a dark spot with V, U, Y or circular shaped cracks [23]. These cracks propagate inside the rail head at a shallow angle to the surface, and grow till 3 – 6 mm deep in the subsurface, before they branch downward transversely [24]. Another characteristic is widening of the running band, as a result of plastic deformation caused by the impact of wheel on the local dip in the rail.



- **Tongue lipping** is identified by the extrusion of thin slivers or tongues of material from the running band of the rail, often extending several millimeters down the gauge face of the rail. Cracks can form below the extruded steel and grow into the railhead in a near horizontal plane. Branches can then form running either up or down, leading to a rail break.

3.1.2.2 Rail corrugation

Rail corrugation is a periodic irregularity on the rail tread like a wave, which is often visible to the naked eye. It gives rise to high dynamic loads between wheel and rail, causing degradation of the ballast, loose fasteners, deteriorated sleepers, pulverized ballast and noise. Rail corrugations are divided into two types depending on the wavelength: short wavelengths from 30 to 80 mm and long wavelength from 100 to 800mm [24]. Short wavelengths corrugation is particularly disturbing because it excites a vibration in the audible frequency range. Figure 13 shows an example of rail corrugation in the Metro of Medellín.



Figure 13. Rail corrugation in the Metro of Medellín.

3.1.3 Wear regimes

Early tests using a twin-disc machine demonstrated that two wear regimes existed [25, 26], which were designated as mild and severe. Later work led to identification of a further regime, designated as catastrophic wear [27, 28]. Figure 14 shows the results from a twin-disc test using a R8T wheel steel against UIC60 900A rail steel. The results are plotted in terms of wear rate (material lost in rolled/mm² contact area) against an index based on work done in the contact $T\gamma/A$, known as the wear index. Where T is tractive force (normal load divided by friction coefficient), γ is the slip at the wheel/rail interface and A is contact area. The contact between wheel tread and railhead falls within the mild regime, while the contact between the wheel flange and rail gauge corner falls in the severe or catastrophic regime.

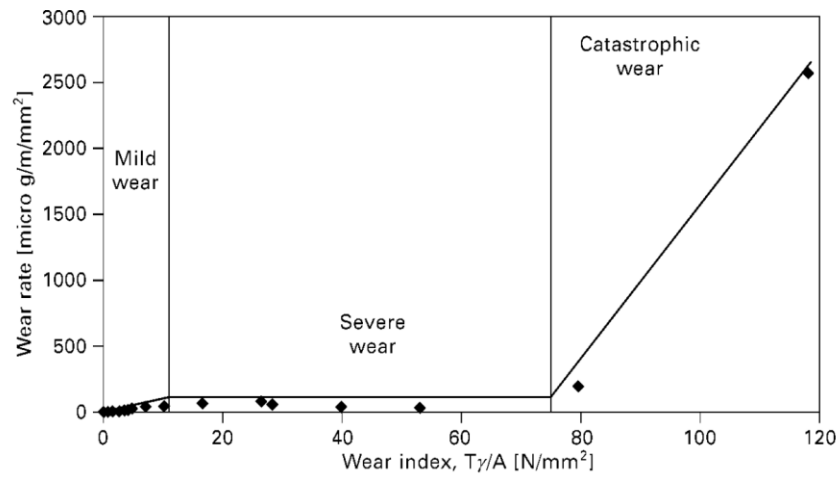


Figure 14. Wear rates and regimes for R8T wheel steel tested against UIC60 900A rail steel [28].

At low wear index in the mild regime, the wheel and the rail are oxidized, turning the surface a rustic brown. A close examination allows observing marks produced by abrasive particles of oxide sheets detached from the surface, see Figure 15a. The results can be compared with field lines, which are evidenced when low slip rate takes place, see Figure 16.

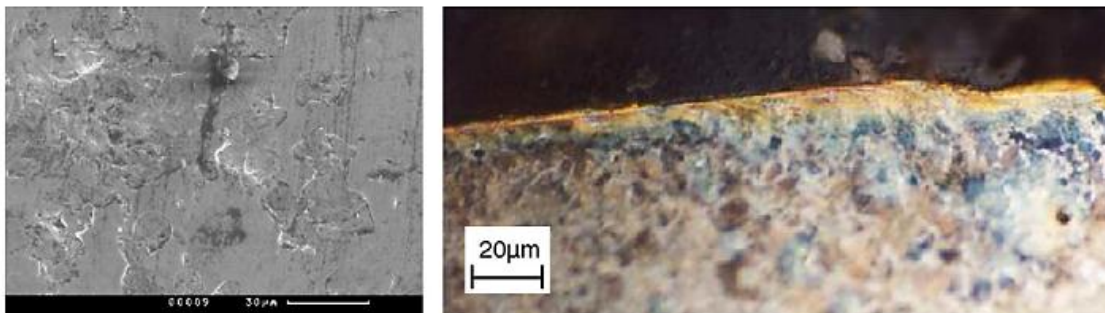


Figure 15. Wheel disc surface run at: (a) $T\gamma/A = 0.21$; (b) $T\gamma/A = 4.1$ [28].

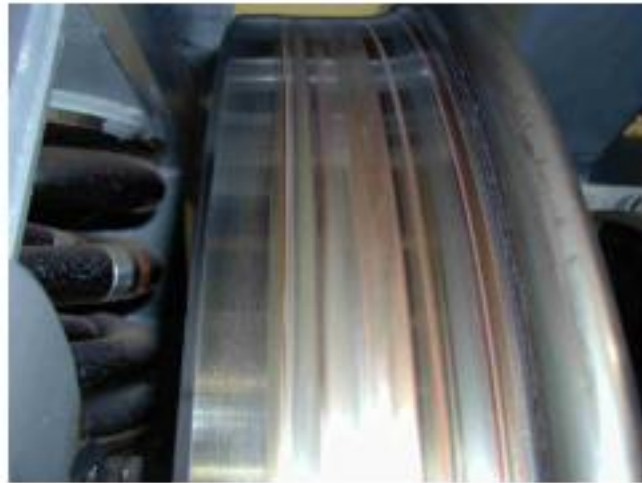


Figure 16. Wheel rolling surface on a full-scale roller rig after 2000 km [29].

When the wear index is increased, the mechanism is altered and ratcheting takes place [29]. As shown Figure 17a, the subsurface morphology exhibits a larger amount of plastic deformation and crack formation is visible, which leads to thin slivers of material breaking away from the surface, see Figure 17b.

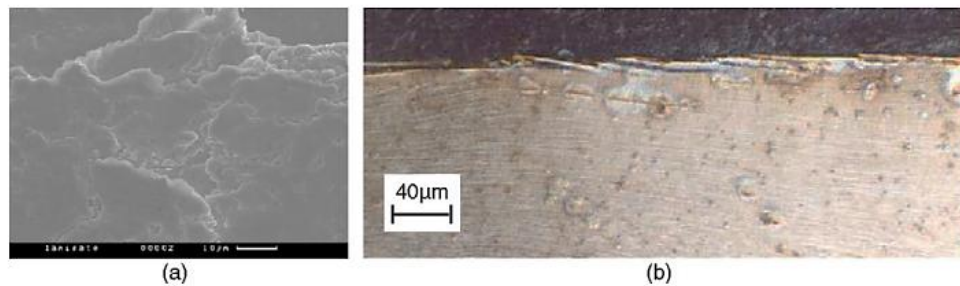


Figure 17. (a) Ratcheting marks (b) Crack formation [29].

When the wear index increases further, several cracks are visible at the wear surface and some of them alter their growth direction. The cracks run parallel to the surface and then turn down into the material causing larger chunks of material break away, See the Figure 18.

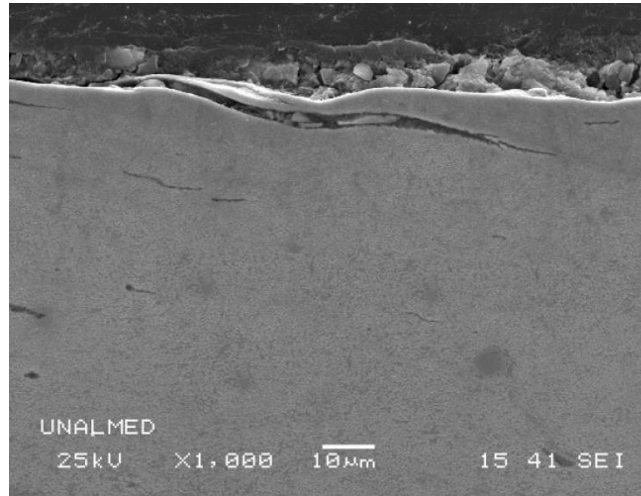


Figure 18. Crack growth in wheel disc

3.1.4 Wear transitions

Lewis and Dwyer-Joyce [28] studied the wear mechanisms and the transition between the regimes. They proposed that the first transition is associated with the beginning of the sliding contact and the second one is a result of temperature effects on the surface.

Figure 19 shows a sliding curve at 1500MPa of contact pressure, where the white dots represent the wear data and the black diamonds the traction coefficients under different slip percentages, also the Carter creep curve is shown for an assumed limiting friction of 0.5. In the beginning of curve there is a high slope and then the friction reaches a limit of 0.5, this transition point represents the change from the partial sliding to the total slip condition. On the other hand, the wear data follow a similar pattern, indicating that at the point of transition from partial slip to full slip a wear transition also occurs.

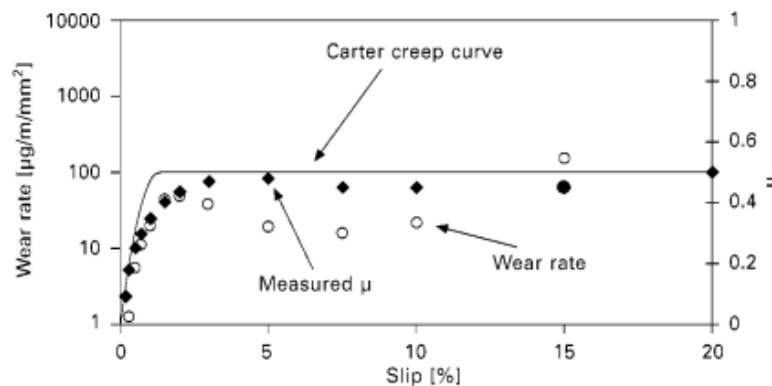


Figure 19. Friction versus slip in the twin-disc contact (for tests carried out at 1500MPa) [28].



During the second transition, another mechanism is initiated, generating higher wear rates. Once the slippage has reached 15% the wear rate increases rapidly. However, the stress state of the smooth surface remains constant due to the normal load and the traction coefficient does not changed either. Clearly the increase of the sliding speed produces a change in the wear mechanism. This change is associated with the increase in temperature in the contact patch, as E.A. Gallardo [30] shows in Figure 20 in which the transition from severe to catastrophic wear occurs between 200°C and 300°C. These temperatures correspond to a drop in yield strength of the carbon-manganese steels, which are the materials used to produce the wheels and rails, see Figure 21.

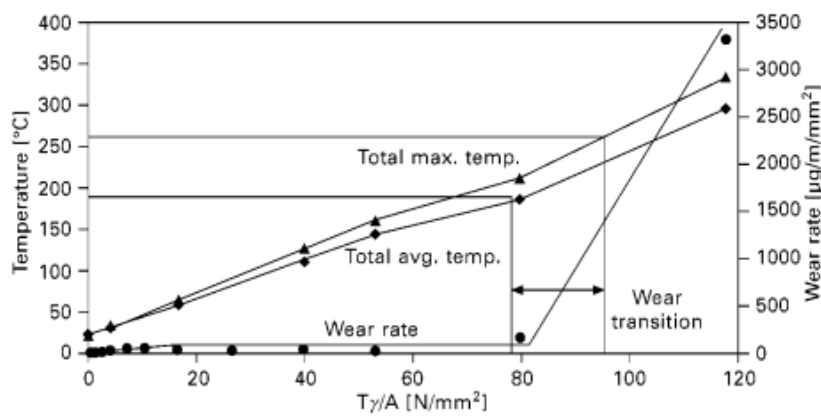


Figure 20. Twin-disc contact temperatures and wear coefficients for UIC60 900A rail material versus R8T wheel material [30].

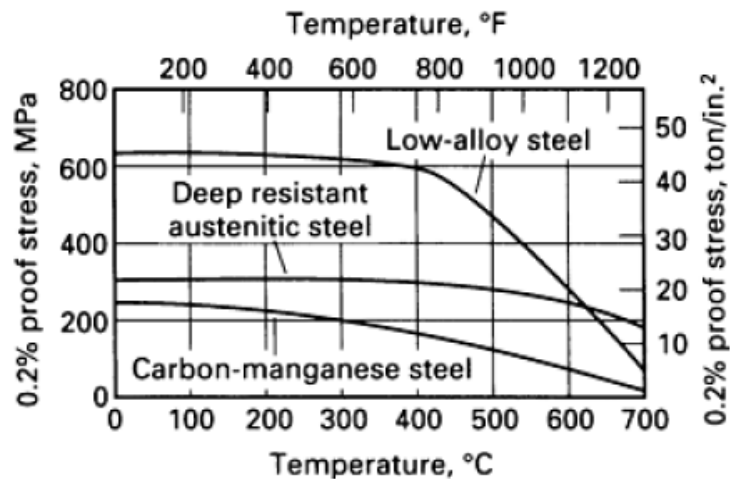


Figure 21. Variation of the yield strength with temperature [31].



3.1.5 Wear modeling

Many experiments have been carried out to explore the wear characteristics of various wheel and rail profiles and materials under different operation conditions, and a number of theoretical and experimental wear laws have been proposed.

It has been proposed that the amount of material worn away from the rail/wheel interface by adhesive, abrasive or fatigue wear is proportional to the load, the distance of sliding, and inversely proportional to the hardness [32, 33, 34, 35]. Equation (1) relates the volume of material worn away with the energy consumed in the contact using a constant called K, which contains the system characteristics like influence of material properties, nature of the wear, contact condition, among other.

$$V = \frac{cIN}{H} = \frac{c}{Hf}(I(Nf)) = k(IF) = KW \quad (1)$$

Where

V: Volume of material worn away,	K: =c/(Hf), wear coefficient.
c: constant,	f: coefficient of traction,
l: distance of sliding,	F: fN, tangential (frictional) force,
N: normal force,	W: Fl, frictional work
H: hardness of material,	

As mentioned above, three main types of wear are observed in the railway systems: Mild (Type I), severe (Type II) and catastrophic (Type III). Clayton [36] and Bolton [37] found experimentally a model to relate the wear regimens with the material loss:

$$\frac{W}{Ad} = m \frac{T\gamma}{A} + C \quad (2)$$

Where

W: Material weight lost,	T: Creep force,
A: Contact area,	γ : Creepage,
d: Distance of rolling,	C: Constant.
m: Constant,	

When the wear rate is mild C=0, while for severe and catastrophic wear C has to be determined by experiments.



The expression of Elkins and Eickhoff [38], called the Derby wear Index, is commonly used. As well as the expressions above, it assumed that the wear rates are related to frictional work done in the wheel–rail contact area.

$$WR = K(T_1\gamma_1 + T_2\gamma_2) \quad (3)$$

Where

WR: Wear rate.

K: wear coefficient.

γ : Slip at the wheel-rail interface.

The wear coefficient (k) can be determined experimentally or by relating field measurements of the wear depth with the mileage for the wheels or the number of wheel passages for the rail. Parameter identification also can be used to obtain K [39].

3.2 Wheel – rail contact

As Figure 22 shows, there are three functional zones at the rail/wheel interface: contact between the central region of the rail head and wheel tread (Region A), contact between the gauge corner of the rail and the wheel flange (Region B), and contact between the field sides of both rail and wheel (Region C).

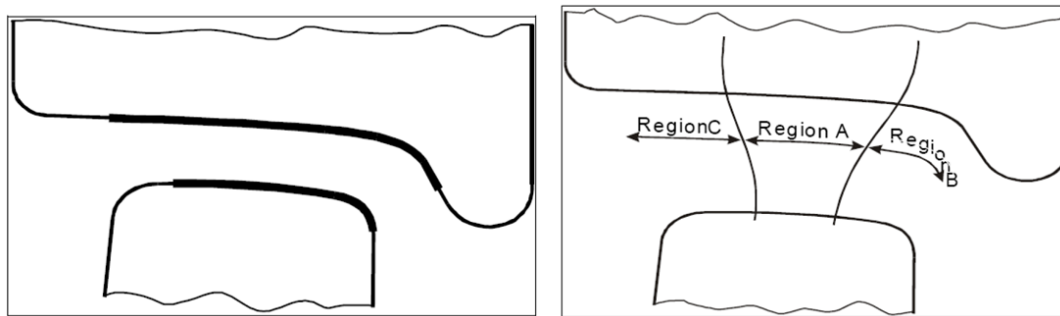


Figure 22. Potential contact zones of the wheel and the rail [19].

The classical theory of contact was developed by Hertz [40] in 1882, when he was a 24-year-old research assistant at the University of Berlin. He demonstrated that the contact area between two non-conformal bodies of revolution would be elliptical and established a method for calculating the semi-axes of the ellipse and the pressure distribution within the contact patch. The Hertz theory is strictly restricted to frictionless surfaces and perfectly elastic solids. Although it does not take into account tangential forces, which are very important in wheel/rail systems, it still provides a valuable starting point for most contact problems and is included in most computer programs which deal with the wheel–rail contact problem.



The contact problem becomes more complex when a tangential force is applied to the contact. This problem is found in literature as rolling with traction [41] and it is very common when the vehicle navigates in a curve and the flange of the wheel is in contact with the gauge corner of the rail. Under this condition, the elliptical contact patch is divided in two zones, adhesion zone and micro-slip zone. The tangential force is higher as the slip rate increases. Once the slip zone reaches the entire contact patch a constant coefficient of friction is found, see Figure 23. In wheel rail contact this relative micro sliding is called creepage and is the most important source of noise in curves.

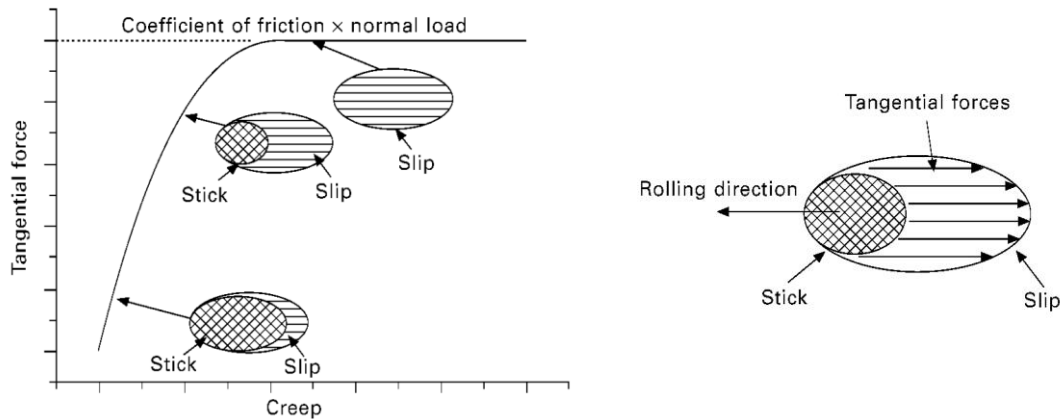


Figure 23. Relationship between tangential force and creep at the wheel- rail contact [42].

To develop creep force a certain amount of slip (creepage) is required. The creepages act in the plane of the contact patch and are related to some dynamic and geometric parameters as the equations (4), (5) and (6) describe for the longitudinal, lateral and spin creepage in case of steady curving respectively [43].

$$v_x = \frac{V_x - r\omega}{V_x} \quad (4)$$

$$v_y = -\alpha \quad (5)$$

$$\varphi = \sin \gamma / r_o \quad (6)$$

Where

v_x : Longitudinal creepage

v_y : Lateral creepage

φ : Spin creepage

V_x : Longitudinal speed of the wheelset

r : Rolling radius of the wheel at the contact point

ω : Rotation speed of the wheelset

α : Yaw angle

γ : contact angle

r_o : Rolling radius of the wheel



An early contribution to the theoretical development was the Carter's creep law, proposed by Carter in 1926 [44]. Carter analyzed the behavior of a locomotive wheel transmitting large traction or braking forces. He used a cylinder rolling on an infinite half-space model to reproduce the longitudinal action. Carter showed that the tangential force is bounded by zero at zero slip and the maximum force given by Coulomb's friction law, see Figure 24:

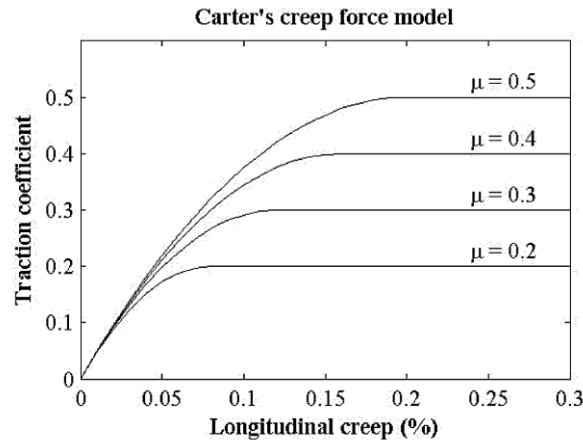


Figure 24. Traction coefficient as a function of creep for different friction conditions according. $R=0.5m$, $a =4m$ [45].

Carter proposed a mathematical model to calculate the contact force under longitudinal creepage.

$$\frac{F_{\xi}}{\mu N_{\zeta}} = \begin{cases} -kv_{\xi} + \frac{1}{4}k^2v_{\xi}|v_{\xi}| & \text{if } k|v_{\xi}| \leq 2 \\ -\text{sgn}(v_{\xi}) & \text{if } k|v_{\xi}| \geq 2 \end{cases} \quad (7)$$

$$k = \frac{4R}{\mu a} \quad (8)$$

Where.

F_{ξ} : Longitudinal force
 N_{ζ} : Normal Force
 k : Carter's creep coefficient

μ : Coefficient of friction
 v_{ξ} : Longitudinal creepage

For small values of creep, the quadratic term in carter's formula may be neglected.

In the sixties, Kalker developed a linear theory based on this approach [46]. Both longitudinal, lateral creep and spin was considered while the contact patch was assumed to be elliptic according to Hertz' theory:



$$\begin{Bmatrix} F_{\xi} \\ F_{\eta} \\ M_{\zeta} \end{Bmatrix} = G C^2 \begin{bmatrix} C_{11} & 0 & 0 \\ 0 & C_{22} & cC_{23} \\ 0 & -cC_{23} & cC_{33} \end{bmatrix} \begin{Bmatrix} v_{\xi} \\ v_{\eta} \\ \phi_{\zeta} \end{Bmatrix} \quad (9)$$

$$c^2 = ab \quad (10)$$

Where.

F_{η} : Lateral Force

M_{ζ} : Spin moment

C_{ij} : Kalker's creep coefficients, $i, j \in \{1,2,3\}$.

v_{η} : Lateral creep ratio

G : Shear modulus

a, b : The semi-axis of the ellipse

Kalker tabulated the creep coefficients C_{ij} as function of the Poisson ratio ν and ratio a/b of the contact ellipse semi-axes.

One of the most important contributions to this field by kalker is a simplified theory suitable for fast computer implementation. In this approach the equations are decoupled by the application of an elastic foundation formulated as mutually independent discrete springs. The implementation of this algorithm is referred as Fastsim [6]. Kalker linear theory is extensively used in practice in rail vehicle dynamics applications, both directly in linear simulations where the creep is sufficiently small and as basis for non-linear extensions. Kalker also provided a numerical implementation using boundary element discretization [47]. This code, called Contact, is often used as reference but requires too much computer time for on-line use in vehicle dynamics simulations. An extension of this method, called WEAR was presented in [14]. It was found feasible to apply for online application in vehicle dynamics simulations for harsh cases such as conformal contact and contact in turnouts [48].

3.2.1 Traction coefficient

In general the tangential forces depend on the normal load, friction conditions, and relative motion between the contacting surfaces. Under total sliding condition the tangential stress (τ) is related to the friction coefficient (f) and normal stress (σ) by the following equation:

$$\tau = f\sigma \quad (11)$$

However, as it was mentioned previously in a rolling sliding contact the elliptical contact patch is divided in adhesion zone and slip zone and the equation 11 is not met. Figure 25 shows the linear relation of the tangential stress in the adhesion zone based on Kalker simplified theory. Due to the tangential stress decreases linearly when the adhesion zone is reached $\tau < f\sigma$ and a new relation is proposed as [49]:

$$\tau = \mu N/A \quad (12)$$



Where μ is the traction coefficient, N is the normal force and A is the contact area and taking into account that $\sigma = N/A$, it is possible to show that $\mu < f$. For this reason in rolling sliding contact the traction coefficient is always lower than the friction coefficient.

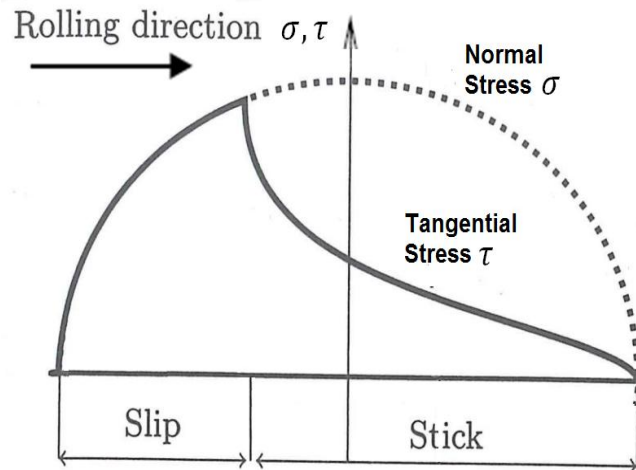


Figure 25. Assumption of distribution of normal and tangential stresses in the wheel-rail contact area.

3.3 Railway vehicles

3.3.1 Bogies

The bogies serve the following functions:

- Support railcar body firmly
- Run stable on both straight and curved track.
- Ensure good passenger comfort by absorbing vibrations generated by track irregularities and minimizing impact of centrifugal forces when train runs on curves at high speed.
- Minimize generation of track irregularities and rail abrasion.

Bogies are classified according to their configuration in term of the number of axles, design and structure of the suspension.

Bogies can be classified into non-articulated and articulated types. Two non-articulated bogies support one railcar body, but one articulated bogie supports the back end of the forward car and the front end of the rear car, as the Figure 26 shows. Despite of the articulated bogie has some disadvantages, such as a complex structure, increased axle load due to the support of one body by one bogie, and difficult maintenance, it offers a lower center of gravity, better ride comfort because car ends do not exceed the bogies, and less effect of running noise on passengers because seats are not over bogies.

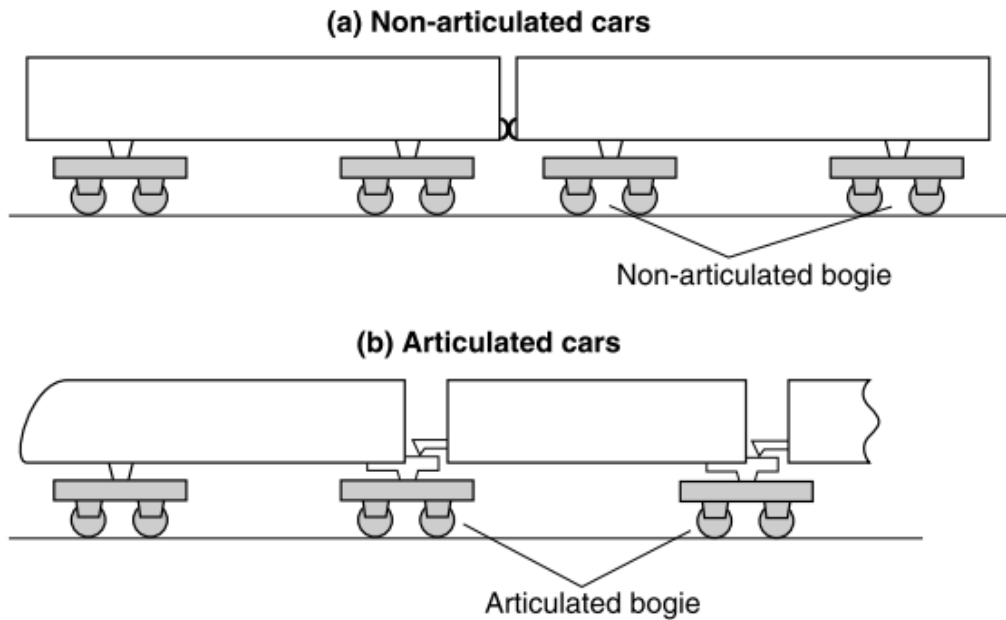


Figure 26. Non-articulated Bogie and articulated Bogie [50].

The bogies can also be classified in terms of the number of axle as bogies B-B, Bo-Bo or Co-Co. Bogies with two axles are classified as Bo-Bo or a B-B, see Figure 27a. The difference between a Bo-Bo and a B-B is that the two axles in a B bogie are coupled together, either by a coupling rod (once common but now obsolete) or because they are both driven by the same motor. On other hand, bogies with three axles are classified as Co-Co, see Figure 27b.

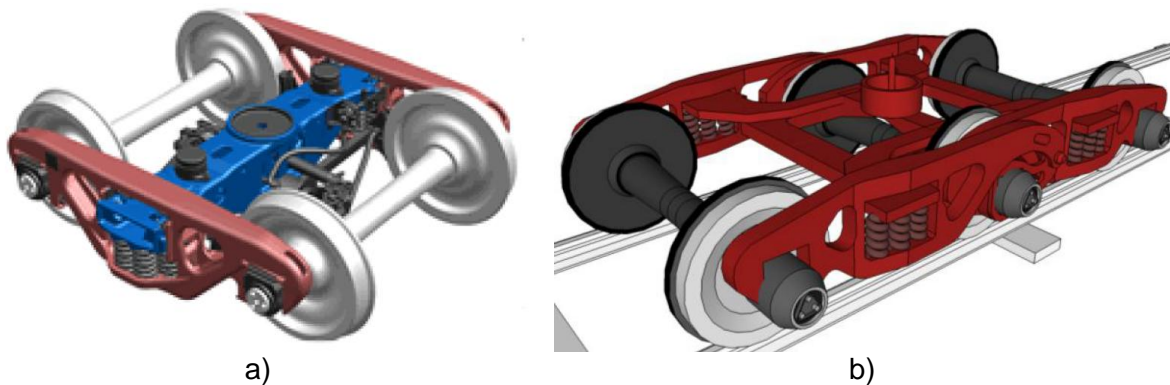


Figure 27. Bogie classification according to the number of axle. a) B-B/Bo-Bo bogies, b) Co-Co Bogies [51]

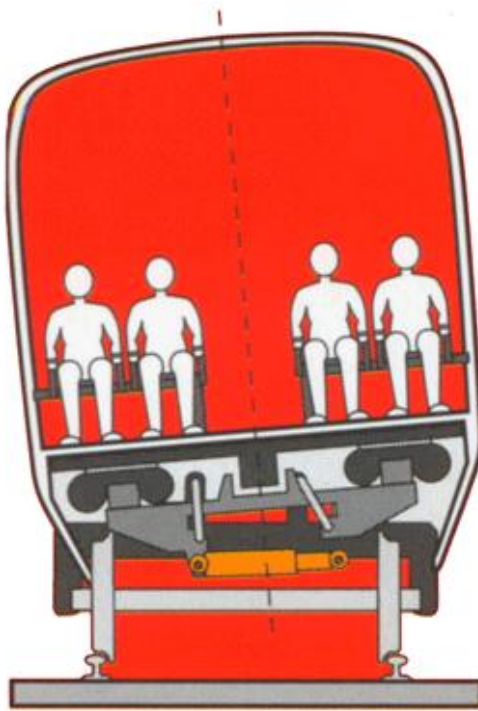
New bogie designs are required to meet the demand for higher speeds, thereby cutting travel times and making trains more competitive with planes and cars. Two types of bogies have been developed to achieve this aim: the tilting bogie, which increases running speed



on curves without effecting running speed comfort, and the steering bogie, which permits higher speeds on curves by minimizing the lateral force on the rail.

3.3.1.1 Tilting bogie

The tilting car has been developed to minimize the effect of the centrifugal force experienced by passengers and permitting the train to travel faster by tilting the body toward the inside of the curve. An example is the SIBI system developed by CAF, see Figure 28a. The SIBI System is an active tilt system which provides rail vehicles with a cant effect in addition to that of the track. A similar technology is implemented in the ICE T ("T" for tilting, DB class 411), which allow to reach a tilt angle of 8°, see Figure 28b. Note that although the tilting car reduces the lateral force on the passengers it does not reduce the lateral force of the vehicle on the track.



a)



b)

Figure 28. Tilting bogie. a) CAF SIBI system (<http://www.caf.es/es>), b) DB class 411 ICE T (<http://www.railsimulator.com/>).

3.3.1.2 Steering bogie

As a train runs on a curve at high speed, the wheels exert high lateral force on the rails causing wear and tear of wheel flanges and rails, and resulting in derailing in extreme cases, see Figure 29b. The steering bogies use the longitudinal creep forces generated between the wheelset and the rail to deflect the longitudinal springs, which create the



bending stiffness. This permits the wheelsets to align to an almost radial position to the curve, as Figure 29a shows. The lateral creep forces are reduced to almost zero, eliminating the flange force and the effect on the rail [20]

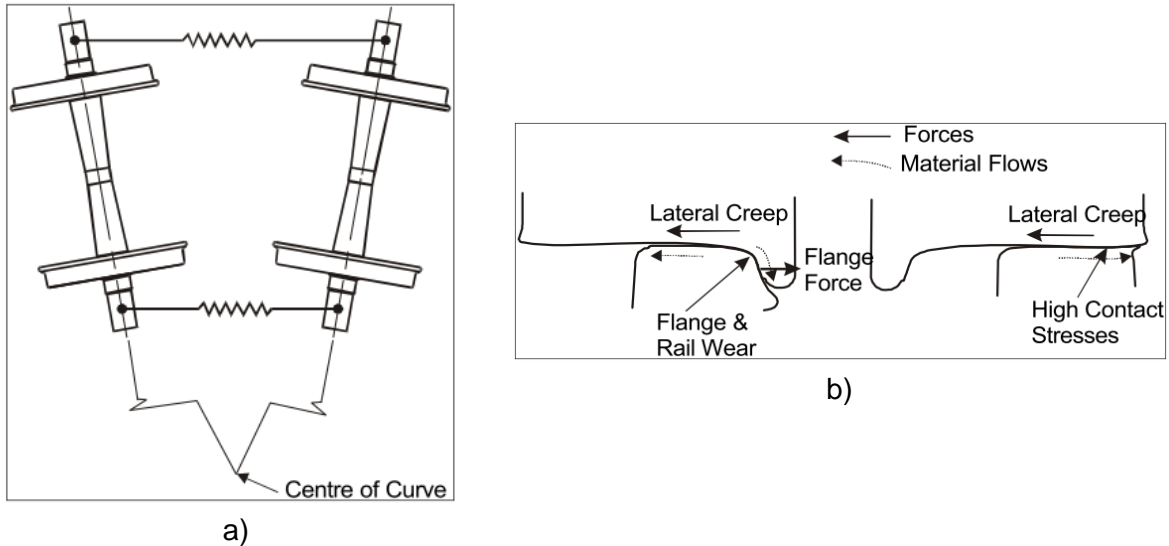


Figure 29. Steering bogie a) Radial Alignment in a Curve, b) Worn Rails in a Curve [20].

3.3.2 Bogie frame

3.3.2.1 Rigid frame Bogie

The rigid bogie frame acts as a single rigid body in the form of “H” shape as Figure 30a shows. This type of frame is not used in heavy haul operations, since it does not leave enough space for springs with adequate carrying capacity and deflection and more importantly the manufacturing cost is too high for heavy haul, due to its complexity and tolerances.

3.3.2.2 Three-Piece bogie frame

The three-piece bogie frame comprises two side frames, each resting in a longitudinal orientation on the axles of the wheelsets. Figure 30b is a sketch of a typical three-piece bogie. The side frames support a cross member, the third piece, called the bolster. The bolster is fitted with a center pivot, which couples the bogie to the vehicle body. The three pieces make the bogie a statically determinate structure and allows the structure to articulate under conditions of track twist. The advantages of this structure for vertical suspension are:

- Efficient accommodation of track twist.
- Suspension springs are limited to two nests offering cost advantages with respect to the number of suspension elements.



- Suspension springs are in a region of the structure where more space is available than at the axle boxes.

A disadvantage is that the side frame forms part of the unsprung mass on the wheelset. Furthermore, the lateral dynamics of the bogie is not optimal.

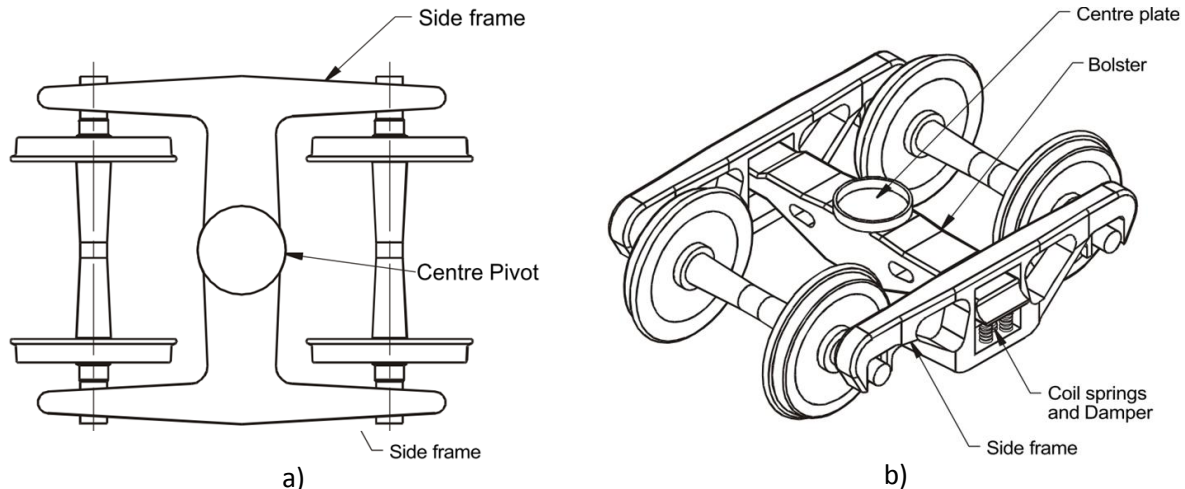


Figure 30. Bogie Frame. a) Rigid Frame Bogie, b) Three-Piece Bogie Frame [20].

3.3.3 Suspension elements

3.3.3.1 Primary suspension

The primary suspension works mainly as vertical suspension and it is responsible for the lateral and longitudinal wheelset guiding. The primary suspension stiffness is critical for the dynamic behavior of the vehicle and the wheel/rail contact stresses on curved tracks.

The primary suspension performs two fundamental functions:

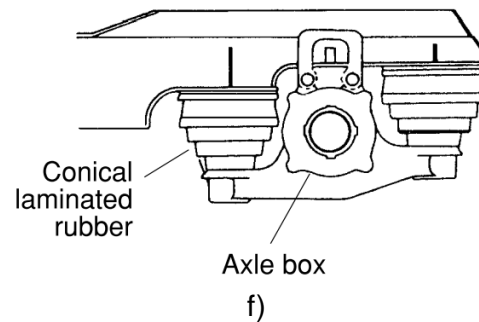
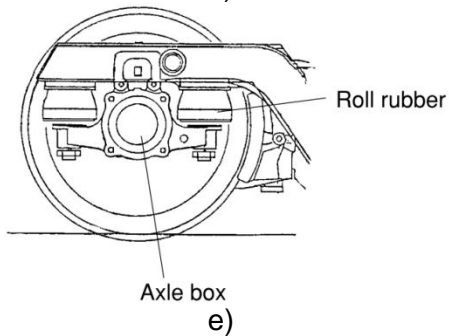
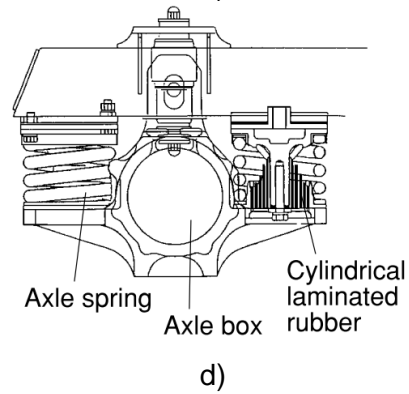
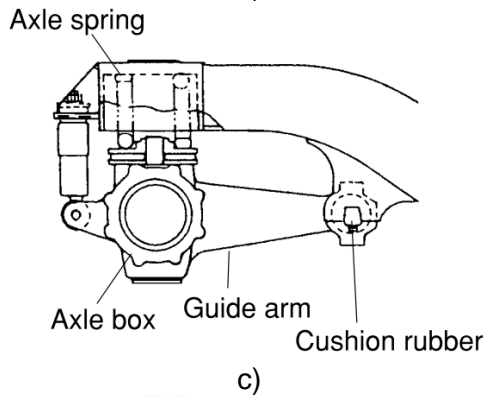
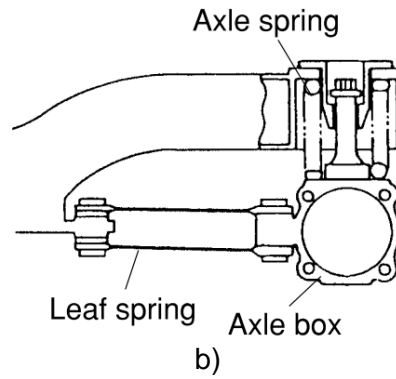
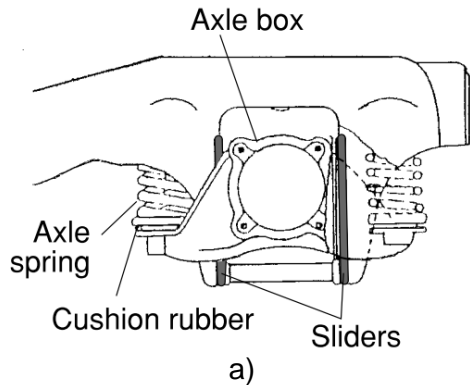
- Reduce the vibrations in the bogie frame, and therefore also reduce the vibration on the different elements installed on it.
- Distribute the loads homogeneously over the wheels, improving the traction, the braking and reducing the derailment risk.

3.3.3.1.1 Axle box suspension

This device supports the axle via the axle box installed in bogie frame. It is a critical component determining the running performance of the bogie, ride comfort and bogie frame construction. Various designs are used, see Figure 31. The pedestal swing spring design supports the axle box using sliders around the pedestal on the bogie frame. Despite of its simple construction, the sliders wear with time, creating play in the suspension and cause wheelset hunting. So, it is not suitable for high-speed operation. While the IS type (Figure 31g) has good cushion rubber stiffness eliminating effectively the



play between the axle and bogie frame. Designs as the roll rubber type, the conical laminated rubber type and the axle beam type allow to simplify the construction and reduce the manufacturing cost.



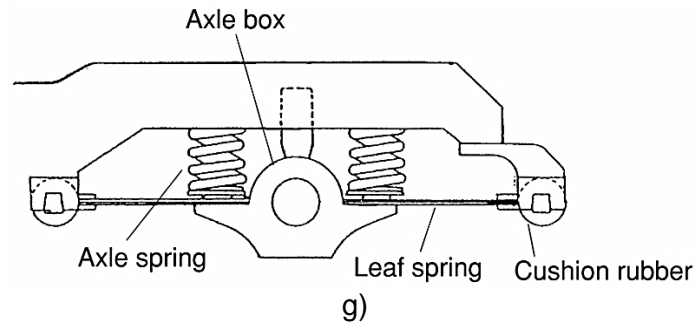


Figure 31. Various Axle box suspensions. a) Pedestal swing spring, b) Leaf spring, c) Axle beam type, d) Coil spring with cylindrical laminated rubber, e) Roll rubber, f) Conical laminated rubber, g) IS type [50].

3.3.3.2 Secondary Suspension

The secondary suspension plays an important role in supporting the body, allowing the bogie to rotate relative to the car body on curves, isolating the body from vibration (including high harmonics) generated by the bogie, and transmitting traction force from bogie to the body.

The air springs are manufactured using elastomeric materials, which have a high failure strain and viscoelastic properties, see Figure 32. Air springs have the following advantages:

- Increase in ride comfort due to pneumatic suspension irrespective of the load conditions
- Reduction in structure-borne noise (vibrations) transmission from the bogie to the car body
- Adjustment of the vehicle height at different loads
- Stabilization of the vehicle at higher speed.

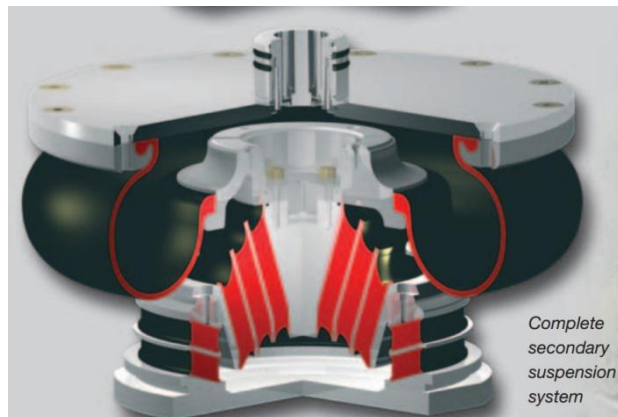


Figure 32. Secondary suspension system. Air spring (<http://www.services-motor.no/>).



3.4 Computer simulation

Using modern computer packages it is possible to carry out a realistic simulation of the dynamic behavior of railway vehicles. The theoretical basis of the mathematical modeling used, is now mature and reliable, and programs, which were often originally written by research institutes, have been developed into powerful, validated, and user-friendly commercial packages. The outputs from these simulations can be set up to provide accurate predictions of the dynamic behavior of the vehicle and its interaction with the track.

3.4.1 Multibody simulation (MBS)

A large number of computer codes have been developed by railway organizations to assist in the design of suspensions and the optimization of track and vehicles. The early packages used text-based interfaces where vehicle parameters were listed in a particular order or using key words to provide the input to the simulation [52]. User-friendly graphical interfaces were added and packages developed to allow engineers to test the effects of making changes to any part of the system and to animate the output; for example, ADAMS/VI-Rail where the user works with a vehicle model through a graphical user interface which allows interaction with the model in the same way as a computer-aided design system, see Figure 33. Other computational packages such as Vampire, Simpack Rail and Gensys use a similar user interface and they are currently widely used. Multibody dynamics theory is used to develop the equations of motion for the system and these are processed by a solver which produces the results of interest.

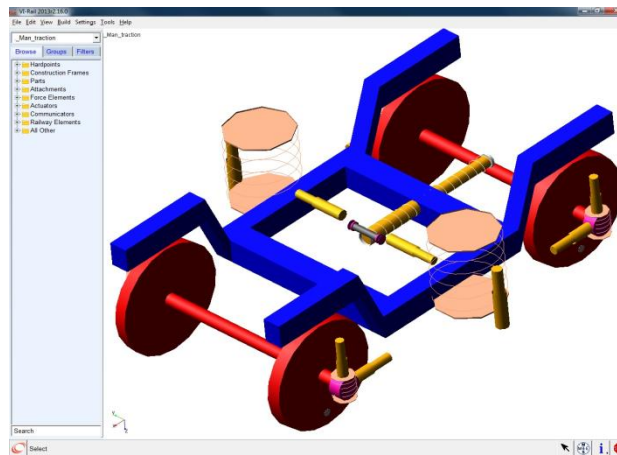


Figure 33. ADAMS/VI-Rail graphical user interface.

Many researches have been performed using the dynamics results provided by multibody simulations. Which allow to identify the kinetic variables such as the position, orientation and derivatives thereof of the wheelset and consequently of each wheel/rail contact pair. This data are used to feed contacts models such as the Hertzian model and Kalker's



simplified theory (FASTSIM) in order to calculate the contact variables (contact points, contact areas, contact forces and creepages).

3.4.2 Wear modeling using multibody simulation

Tomas Jendel in 2002 [53] used GENSY MBS software to validate a wear prediction tool applied to a vehicle operating at the commuter rail network in Stockholm. The wear modeling is based on Archard's wear model and the results were compared with laboratory measurements, corresponding to about 200,000 km of running distance. Figure 34 shows that simulated and measured worn wheel profiles are in good agreement, meaning that the wear prediction tool predict successfully the life-time wear of a wheel. A similar research was performed by M. Ignesti et al. in 2012 [54] using Simpack Rail to develop a predictive model for the wheel and rail evolution due to wear. However, during a simulation a specific point on the rail is in contact only one time with the wheel, while the wheel is in contact many times with the rail. This situation that the wheel to wear much faster than the rail. M. Ignesti proposed a model based on a discrete process with different time scales between the wheel and the rail. The wheel time step is based on the kilometers traveled by the vehicle, while the rail time step is based on the total tonnage corresponding to the number of vehicles traveling on the track. So the wheel profile will be updated more frequently than the rail profile.

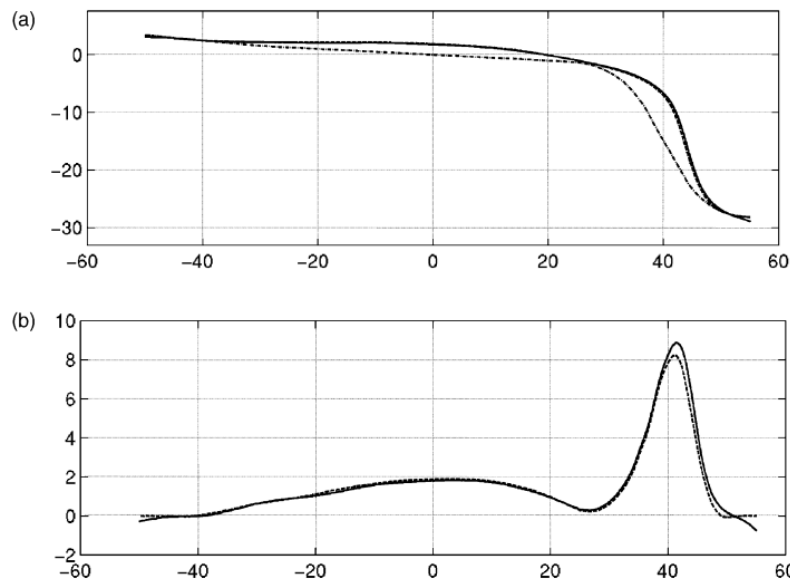


Figure 34. Comparison between simulated and measured wheel profiles after 200,000 km running distance: simulation (solid line), measurement (dashed line). The initial wheel profile is also shown. (a) Wheel profiles, (b) wear distributions (decrease in wheel radius). Measurements are in mm [53].



A research carried out by F. Braghin et al. in 2006 [29] allowed to predict the wheel profile evolution through numerical modeling. Results obtained from multibody simulations were used in a wear model based on Derby wear indexes (equation (3)), where the wear coefficient was calculated based experimental results obtained with a twin disc test machine. The wear prediction model was validated using full-scale experimental tests carried out on a single mounted wheelset under laboratory conditions and implemented to predict the evolution of the wheel profile during standard service in an ETR500 Italian high speed passenger vehicle. Figure 35 shows the results of the numerical simulations performed using the wheel profile wear prediction model. The results of material loss are in very good agreement with the measurements; the estimated total tread wear amount after a mileage of 10,500 km is 5% smaller than the experimental one, but comparing the experimental and the numerical total flange wear amount, an overestimation of about 30% is obtained by the prediction model. However, the wheel wear prediction model is able to correctly foresee that about 60% of the total flange wear occurs in the first 2500 km.

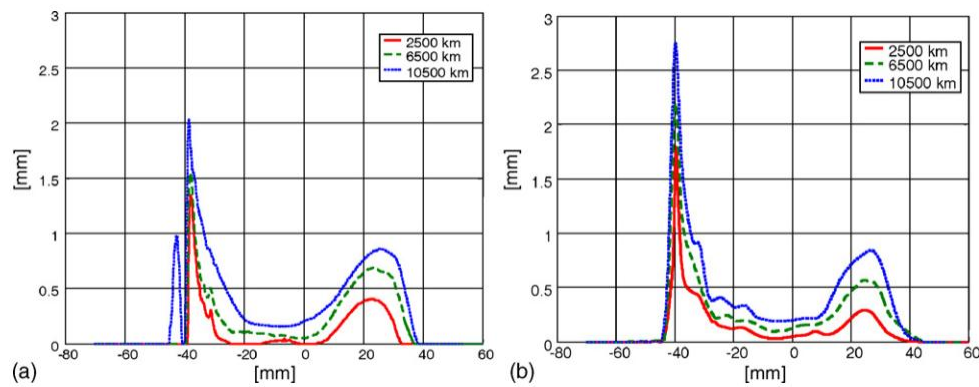


Figure 35. Comparison between (a) experimental and (b) numerical transversal profile wear depths at different mileages [29].

Figure 36 shows results from the simulation of the service wear life of a wheel. Braghin calculated the amount of abraded material (in grams) on the whole wheel profile corresponding with the three identified wear regimes (mild, intermediate and severe wear) for every 25,000 km of mileage and the continuous evolution of the flange thickness parameter S_d with mileage. These results are very important since they allow to identify the mileages at which the wear mechanism changes. This allows to set-up an optimized maintenance (re-profiling) strategy for each face in the wheels life, and therefore to increase the wheels life time.

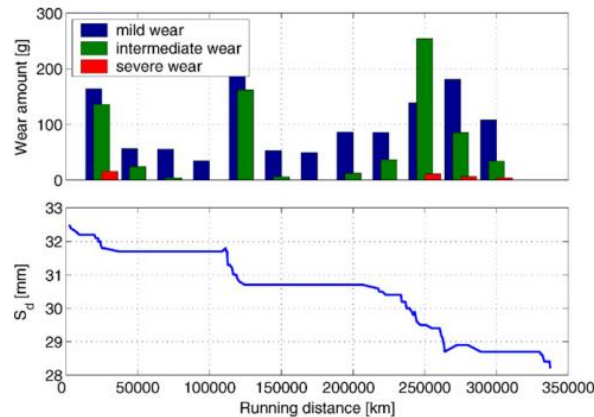


Figure 36. Numerical evolution of flange thickness control parameter S_d with mileage (lower) and amount of abraded material for each wear regime with mileage (upper) [29].

Y.Q. Sun et. al. also carried out multibody simulations using Vampire in 2010 to predict the wheels wear of a railway vehicle passing through a railroad switch. The results show the effect of operational conditions, such as the vehicle velocity in the wheel wear rates [55].

3.5 Friction modifiers and lubrication system

3.5.1 Friction modifiers

Friction modifiers are materials that are added in wheel and rail interface to create a third body with desired properties.

They can be divided into three categories [56]:

1. Low coefficient of friction modifiers (LCF), with a target coefficient of friction of 0.2 or less are used to reduce friction at the wheel flange/rail gauge face interface. Solid lubricants are widely used because they can provide a thicker layer than liquid or grease lubricants under the same pressure and relative slippage; Figure 37 shows a solid lubrication system develop by Kelsan.
2. High friction modifiers with intermediate ranges of coefficient of friction (from 0.2 to 0.4) are used at the wheel tread/top of rail interface to reduce the rolling resistance of freight cars, control short pitch corrugation growth, reduce hunting, and reduce wheel squeal.
3. Very high friction modifiers (friction enhancers) are applied to increase locomotive adhesion and improve the braking performance.

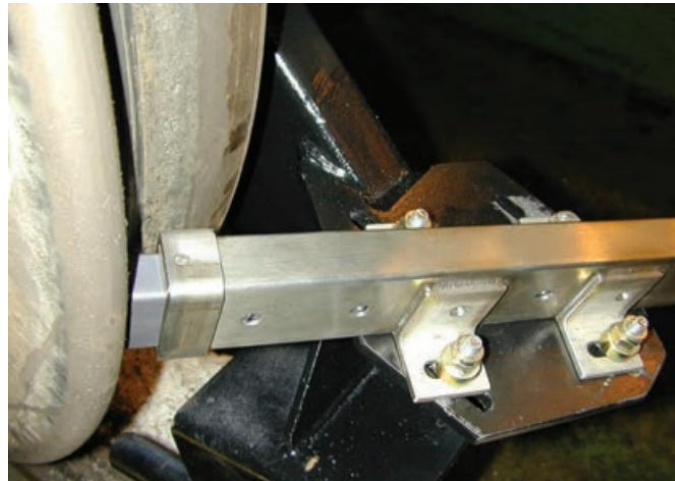
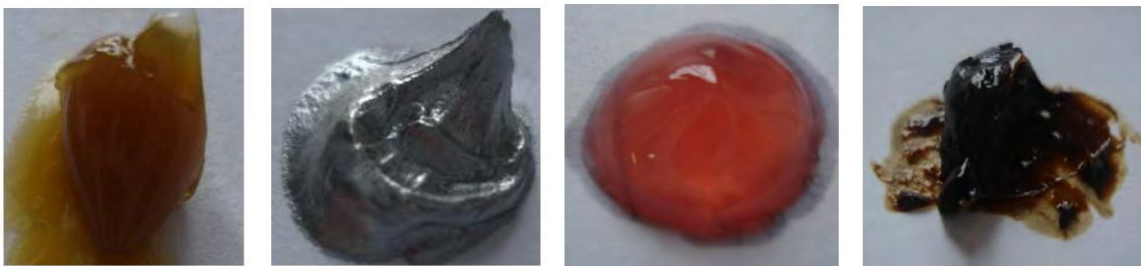


Figure 37. KELSAN wheel flange solid lubrication (<http://www.kelsan.com>)

The high friction modifiers as well as very high friction modifiers, include a high content of abrasive particles which produce micro abrasion in the contact interface ensuring a high friction coefficient. Greases with high viscosity are most commonly used for wheel/rail systems, they are composed of a base oil, additives, soaps, thickeners, and friction modifiers among other components; Figure 38 shows the aspect of commercial lubricants used in wheel rail contact. Metal soaps are currently used in lubricating greases to achieve temperature stability. Calcium soap greases are suitable for lower temperature conditions. Calcium greases also have excellent hydrophobic properties while lithium soap greases have a far better high temperature stability, but lack the same hydrophobic properties as calcium soap greases [57]. The most important properties of greases are the specific soap type, the presence of solid lubricants, and the suitability for the applicators. The water resistance allows the grease to stick to the flange or top contact zone even in adverse weather conditions.



- a) Side lubricant (stationary)
- b) Lubricant for the top of rail (stationary)
- c) Ossagol V Grease (on board)
- d) Whitmores bio-rail (stationary)

Figure 38. Aspect of several lubricants used in wheel rail systems [1].



3.5.2 Lubrication Systems

There are generally two types of lubrication systems:

3.5.2.1 Lubricants delivery systems on-board

On-board systems apply grease or solid lubricant to the wheel flange, which is then transferred to the gauge side of the railhead. The lubricant flow is usually controlled by the wheel revolutions. The lubricant may be applied one sided or to both wheels. Grease is applied to the wheel through a nozzle, as Figure 39a shows. Wheel flange lubricators for solid lubricants use different application systems. For instance, solid lubricant in rolled tubes is applied under pressure to the wheel flange by a special device, see Figure 37.

3.5.2.2 Stationary rail lubrication systems

The units are placed in the track and apply a liquid stream to the rail flange or tread according to the number of axes, rail squeal, time, and others factors. Figure 39b shows an example of a stationary rail lubrication system. The disadvantages of stationary delivery systems are the high maintenance costs due to the need to align and properly clean delivery nozzles. The effectiveness is affected by the location of the lubricator with respect to the curve and the viscosity of the grease at different temperatures.



a)



b)

Figure 39. Lubrication systems. a) Lubricants delivery systems on-board, b) Stationary rail lubrication systems.

**OBJECTIVES**

4.1 General Objective

The general objective of this thesis is the identification of the influence of rail lubrication on wear and energy dissipation in the wheel/rail contact interface.

4.2 Specific Objectives

- To install a commercial lubrication system in a specific section of the Metro of Medellin tracks.
- To develop a railway vehicle and track multibody model.
- To calculate the energy consumption under different friction conditions using the results from dynamics analyses.
- To analyze field energy consumption measurements in order to compare them with the simulation results.
- To calculate wear rates in the Metro of Medellin system under different friction conditions.

**METHODOLOGY**

To investigate the influence and the benefits of a lubrication system, a comparison was made of the measured energy dissipation in the track and the energy dissipation obtained from multibody simulations. The detailed methodology is described as follows:

5.1 Lubrication system selection and installation

In order to compare the energy simulation results using the multibody modeling with field energy measurements under different friction conditions, a lubrication system was installed in a curve of the Metro of Medellín Tracks.

5.1.1 Selection of the lubrication system

Several commercial lubrication systems were evaluated in order to select the proper system to be installed in the Metro of Medellín.





The power plays an important role when a lubrication system has to be selected because it is required to pump the friction modifier (FM). The energy demand is related to the shear stresses, velocity, flow and the time required to pump a certain amount of FM. Table 1 shows the results of the comparison among a number of commercial lubrication systems. According to this information, it is possible to conclude that Hy-Power, Lincoln and QHirail systems are adequate to pump most of the greases and FM's, since they provide enough power for the pumping operation. Despite the power of Hy-Power and Delimon is unknown, they are able to pump FM with high consistency (NLGI of 2). However, Delimon Statrack is not suitable to properly pump high viscosity friction modifiers since it is recommended for greases with NLGI 00. Therefore, the lubrication systems Hy-Power, Lincoln and QHirail are more versatile and can pump all kinds of FM's.

On the other hand, although the train sensors of the different lubrication systems analyzed are similar (train counters, noise, time and humidity), the mechanical sensor used by QHirail is not recommended since it requires higher maintenance. Accordingly, the Hy-Power and Lincoln are preferable to use as a delivery device for the Metro of Medellín.

The Hy-Power system was selected due to the good properties of the Sintono Terra HLK as friction modifier. According to the manufacturer, it is a biodegradable ester-based friction modifier, composed by aluminum-silicon, copper and molybdenum disulfide particles.



Table 1. Summary of analyzed lubrication systems.

CHARACTERISTICS	LUBRICATION SYSTEMS.			
	HY-POWER	DELIMON STATRACK 1500	QHIRAIL LUBRICURVE 50	LINCOLN 85565
GENERAL VIEW				
TYPE OF DELIVERY DEVICE	Four holes on the top of the rail	Two or four grease dispensing units	Two or four grease dispensing rectangular plates with grooves for the grease flow	Two rectangular plates with several nozzles to deliver the FM to the head or gauge
POWER	N/A	600W	110W	N/A
DEPOSIT CAPACITY	25kg	8L	25kg	15 L
DISTRIBUTION SYSTEM AND PUMP	Pump control by pulses 1.4cm ³ per pulse.	Pump control by pulses	Simple valve no return	SSV valve
TYPE OF CONTROL	Train accelerometer sensor	Train counter, noise sensor	Mechanical sensor located on the rail	Train and axle counter
LUBRICANTS AND FM TO BE APPLIED	Sintono Terra SKRE Sintono Terra HLK (NLGI 2)	N/A (NLGI 0)	Whitmore Biorail (NLGI 3)	N/A (NLGI 2)



5.1.1.1 Hy-Power system description

The lubrication system provided by Hy-Power uses a vertical pump with an electrical actuator installed, shown in Figure 40. The pump produces a push load up to 1300 N pumping an equivalent of 1.4cm³ lubricant to the top of the rail.

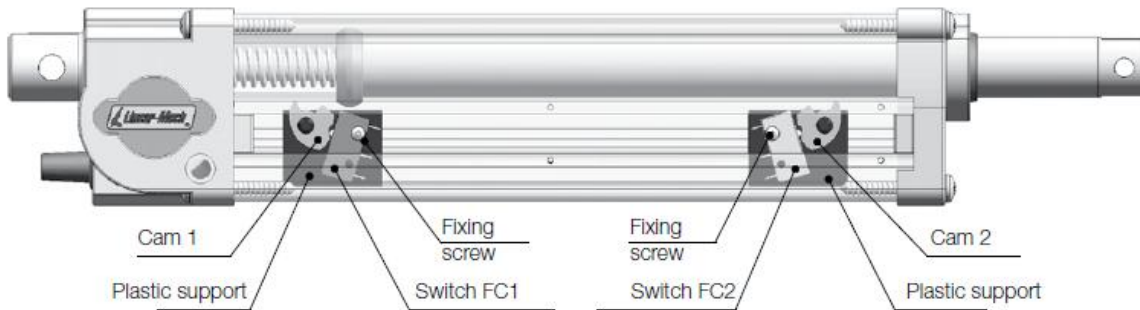


Figure 40. Hy-power actuator (www.linearmech.com)

The control system is composed by an acceleration sensor and a control unit programmed by the user with the desirable number of vehicles and pumping pulses (see Figure 41). The accelerometer detects the passage of the vehicles and sends a signal to the controller, which activates the pump when the counter reaches the established number by the user.



a)



b)

Figure 41. Control system: a) Accelerometer sensor, b) Controller device.

To deliver the lubricant to the top of the rail 4 transverse holes are drilled in each rail, spaced 47 cm to each other. The holes are connected to the pump through hoses and two distribution valves ensuring that the same amount of lubricant flows to each hole. Figure 42a and b show the distribution system and a hole on the top of the rail, respectively.



a)

b)

Figure 42. a) the distribution system b) a hole on the top of the rail.

5.1.2 Installation of the lubrication system

To identify the proper place to install the Hy-Power lubrication system, data related to the wear rates in all the curves of the line B were analyzed. Table 2 shows the results of the wear analysis performed by J.F Santa [1]. According to this information, the most appropriate curves for installing the lubrication system are C22, C19, C12, C11, C6, C4 and C3, since these show severe wear rate conditions and using a friction modifier may contribute to increase the lifetime of the rails.

Table 2. Wear rate calculated for the all curves in the line B.

Curve	C22	C21	C20	C19	C18	C17	C16	C15	C14
HR	0.29	0.12	0.05	0.24	0.05	0.01	0.07	0.03	0.17
LR	0.13	0.02	0.03		0.03		0.04	0.05	
RC	596	496	364	754	600		360		

Curve	C13	C12	C11	C10	C9	C8	C7	C6	C5
HR	0.03	0.37	0.43	0.05	0.07	0.19	0.02	0.33	0.07
LR	0.03	0.08	0.06		0.05	0.11	0.03	0.05	0.04
RC		300	304		304	300		304	300

Curve	C4	C3	C2	C1
HR	0.39	0.41	0.11	0.1
LR	0.05	0.32	0.07	
RC	300	200	304	

Severe	WR > 0.2
Medium	0.06 < WR < 0.2
Mild	WR < 0.06

Curve 4 was selected to install the commercial lubrication system since this curve provides enough clearance in the field side. Unlike the other curves which are located on a viaduct,



curve 4 is on ground level, see Figure 43. This characteristic allows performing the installation and maintenance task in an easier way.



Figure 43. Metro of Medellin tracks. a) Not elevated track b) Elevated track.

The installation process was performed by a Hy-Power technician. Once the lubrication system was installed, a tuning procedure was carried out in order to determine the correct amount of vehicles and pumping pulses. To such an end, iterative tests were performed using an empty vehicle. Initially, the controller device was set in 3x1 (three pumping pulses per vehicle), but when the vehicle stopped in the station the wheels slipped. After test the combination of 2X3 (two pumping pulses every three vehicles) was selected.

5.2 Friction coefficient measurements

The coefficient of friction (COF), at the wheel/rail interface of the Metro of Medellin in line B was measured in the field using a hand-pushed tribometer developed by the Tribology and Surfaces group at the National University of Colombia, shown in the Figure 44a. The measurements were made in curve 4, where the stationary lubrication system is located (see Figure 44b). Three friction conditions were evaluated: Dry, HLK, and Post-HLK. The latter condition corresponds to the case when the supply of FM ends but there is still a remnant layer on the track. Detailed information is presented by Areiza in her master's thesis [58].

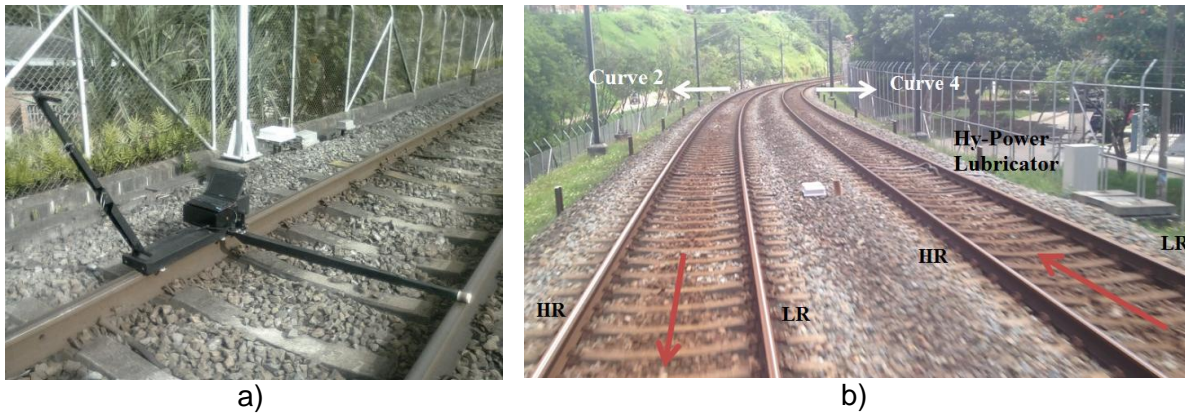


Figure 44. a) Hand-pushed Tribometer, TriboMetro FR-101, b) Curve 4. [58]

5.3 Energy measurements

The measurements of the energy consumption were performed on board of a vehicle of the Metro of Medellín, in the curve 4. The measurements were made using a waveform recorder, WR300® from Graphtec, shown in Figure 45. This device records the voltage and the current taken from the overhead lines, the time, the velocity and the location of the vehicle. Each measurement was performed twice with the same vehicle within a specific hour to keep a similar passenger load and weather conditions in each test.

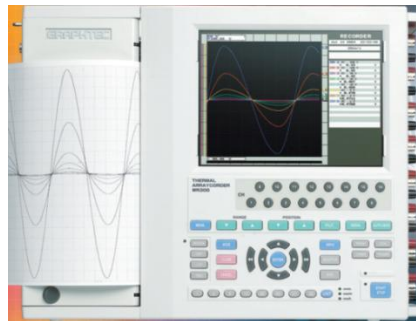


Figure 45. The waveform recorder, WR300, used to measure the electric energy consumption [9].

In order to compare the energy consumption from measurements done with a slightly different velocity profile, it is proposed to subtract the kinetic power, the potential power and the drag power from the total power (see Equation (17 below)). The remaining power (P_{rest}) is dissipated in the wheel/rail contact, the bearings, the gears, the dampers, and the engines. These powers are unknown and cannot be measured. However, it is assumed that in P_{rest} , the largest part should be dissipated in the wheel rail contact. Moreover, all these powers depend only on the vehicle and not on the rail lubrication, with the sole exception of the contact power. It can therefore be assumed that the difference in P_{rest} between the different runs is solely due to the wheel/rail contact dissipation.



Below are the equations to calculate the powers.

$$P_{tot} = I_{red}V_{red} \quad (13)$$

$$P_{kin} = mVa \quad (14)$$

$$P_{pot} = mgV(dh/dx) \quad (15)$$

$$P_{drag} = \rho_{air}A_fC_DV^3 \quad (16)$$

$$P_{rest} = P_{tot} - P_{kin} - P_{pot} - P_{drag} \quad (17)$$

Where

P_{tot} : Total electric power consumed by the vehicle.

P_{kin} : Kinetic power of the vehicle.

P_{pot} : Potential power of the vehicle.

P_{drag} : Power consumed by aerodynamic drag

P_{rest} : The remaining power

I_{red} : Current consumed by the vehicle

V_{red} : Catenary voltage

Δt : Time step

m : Vehicle mass

V : Vehicle velocity

a : Vehicle acceleration

g : Acceleration of Gravity on earth's surface

dh/dx : Height-distance rate

ρ_{air} : Air density, 1.09 [Kg/m³]

A_f : Frontal Area of the vehicle.

C_D : Drag coefficient, 0.81.

5.4 Multibody model development

5.4.1 The vehicle model

A 3D multibody model of a railway vehicle implemented in the software package VI-Rail ADAMS was developed in collaboration with the Metro of Medellín, who provided the technical documentation and experimental results. The vehicle is comprised of three passenger coaches, referred to as A, R and B, of which the first and the last host the engines and apply the traction, as the Figure 46 shows.

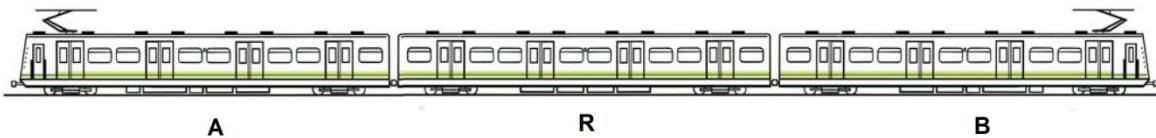


Figure 46. The vehicles model in VI-Rail.

This vehicle reaches a maximum speed of 80 km/h, is powered by 8 engines of 205KW each, while the catenary electric tension is 1500V CC. The dimensions of the car body are 3.2x22.8x3.8 meters (width/length/height) and its mass is 49.9 ton, 44.0 ton and 49.0 ton for the A,R and B coach respectively.



Figure 47 shows the bogies of the Metro of Medellín, which are non-articulated bogies with two axles (Bo-Bo type) and the bogie frame is a single rigid body in the form of “H”. The central pivot and the air springs support the car body loads, which are transmitted to the suspension element located in the axle box.

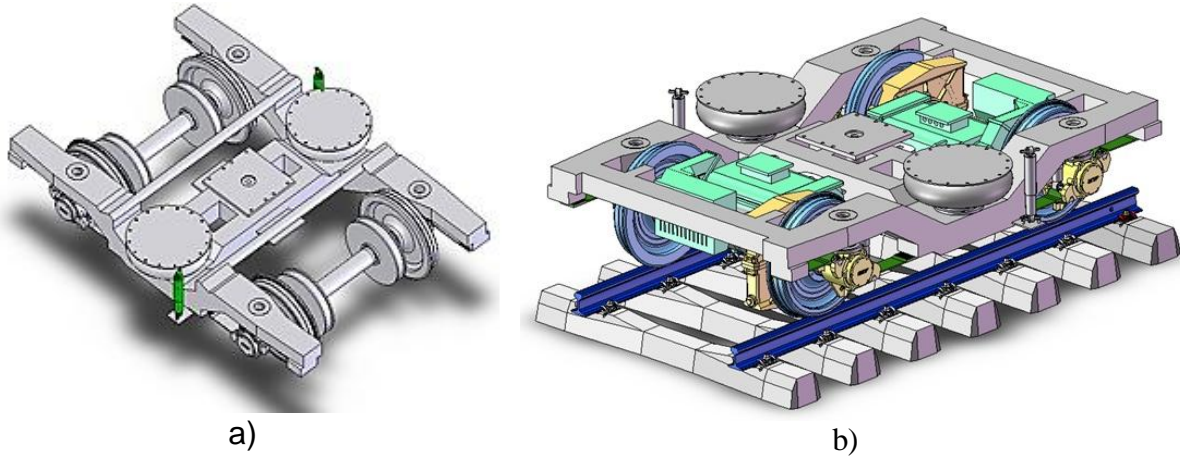


Figure 47. Bogies of the Metro of Medellín. a) Bogie of the trailer coach, b) Bogie of the engine coach [59].

The primary and secondary suspension has been modeled in detail including non-linearities such as in the bumpstops and the bushings. The primary suspension is composed by two nested coil springs, two bushings, one damper and two guide bars as the Figure 48 shows. The latter were modeled using a suspension element. The vertical loads are supported by the coil springs and the longitudinal and lateral loads by the guide bars and bushings, the vertical damping is provided by one damper.

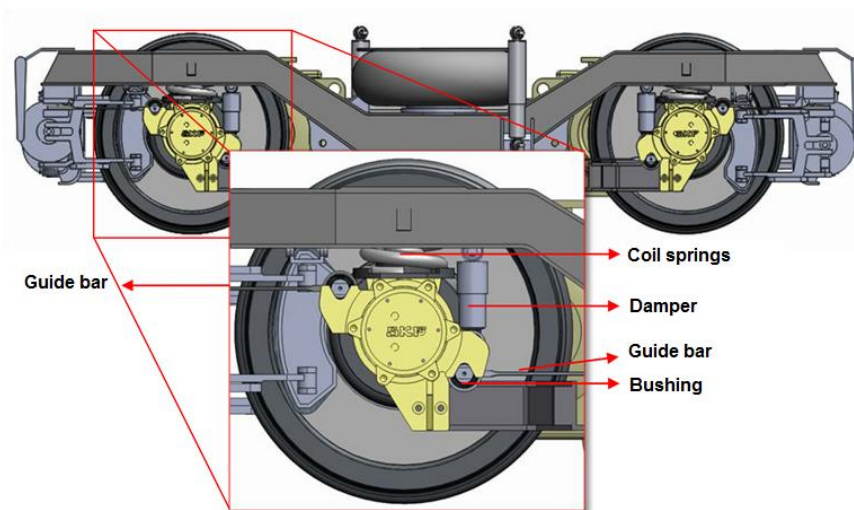


Figure 48. Primary suspension arrangement in the Metro of Medellín [51].



The secondary suspension is composed by two air springs located in the middle of the frame, which were modeled using a suspension element and one damper. For the central pivot, two bumpstops were used to restrict the displacement of the car body in the longitudinal and lateral direction. Moreover, the frame is connected with the car body through two vertical dampers and one lateral damper.

Figure 49 shows the VI-Rail model of one bogie, Figure 50 shows a general view of the assembled model and Table 3 shows the values of the particular parameters of an engine coach.

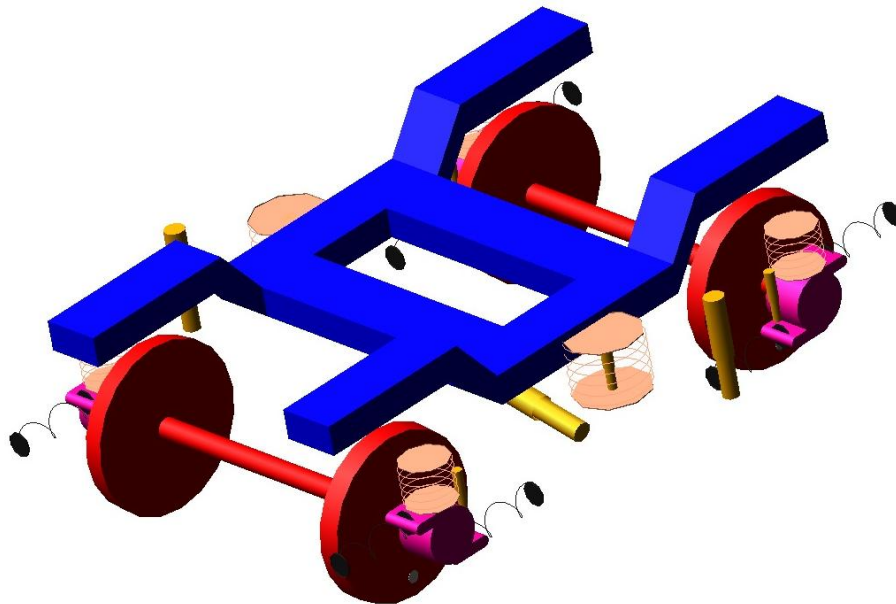


Figure 49. Bogie model in VI-Rail Adams.

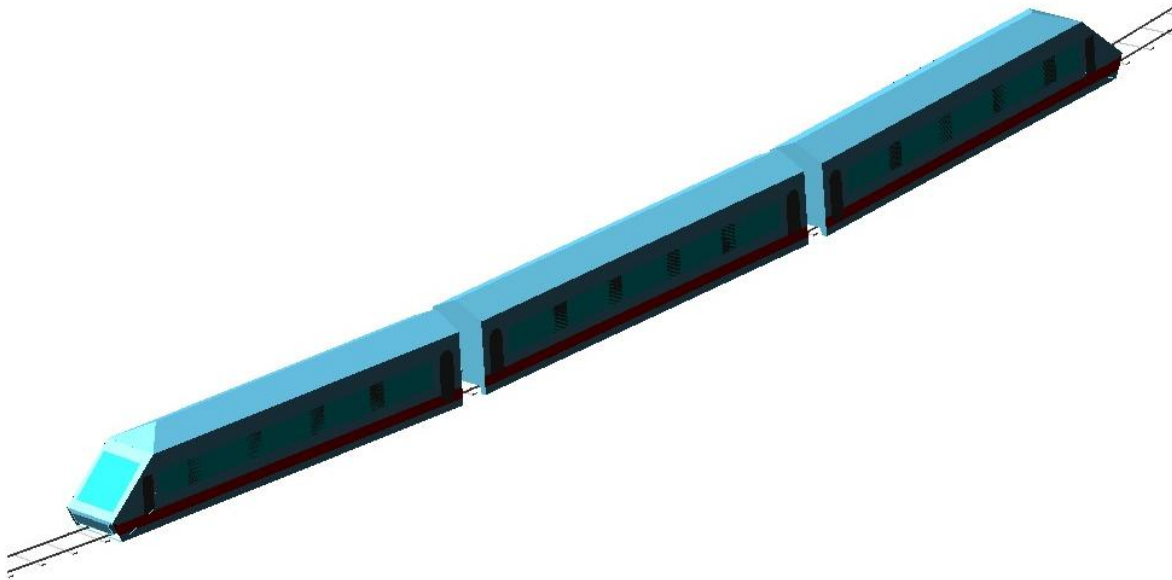


Figure 50. Metro of Medellín vehicle model in VI-Rail ADAMS

Table 3. Vehicle parameters [60].

Element	Quantity	Value	Unit
Mass			
Car body	1	24486.36	kg
Bogie frame	2	6102.44	kg
Motor	4	5551	kg
Electromagnetic brake	4	704	kg
Traction link	2	–	kg
Axle–wheel set	4	7083.52	kg
Stiffness			
Linear	1	$k_A = 1.00$	kN/mm
Nonlinear	20	Array	kN/mm
Shear	8	$k_x = 2.16$	kN/mm
		$k_y = 2.16$	kN/mm
		$k_z = 12.16$	kN/mm
Axis direction	2	0.08	kNm/s
Air spring with auxiliary rubber stack	4	$k_z = 4.52$	kN/mm
		$k_y = 1.04$	kN/mm
Nonlinear damper	13	Array	kNm/s
Bushing	36	$k_x = 67.32$	kN/mm
		$k_y = 36 \times 10^{-5}$	kN/mm
		$k_z = 72 \times 10^{-6}$	kN/mm
		$k_\theta = 36 \times 10^{-5}$	MNm/rad
		$k_\phi = 2 \times 10^{-6}$	MNm/rad
		$k_\psi = 1 \times 10^{-5}$	MNm/rad
DOF	120	–	–
Nonlinear conicity		Array	–



Due to the important role traction plays in the tangential forces and creepages, a moment of force was included in each wheel in order to reproduce the vehicle's acceleration curve. To such an end, the equation of the velocity curve under dry condition was derived and the applied moment per wheel is calculated as:

$$M = \frac{ma(t)R}{16} \quad (18)$$

Where

- m : Vehicle mass
- $a(t)$: vehicle acceleration
- R : Wheel radio

5.4.2 The track Model

The section of the line B between the San Javier and Santa Lucía stations was modeled. This section is composed of two straight lines and the curve 4 (see Figure 51). The curvature radius is 300 m, the track gauge is 1435 mm and the cant is 150 mm, the total length of the track is 765.4 m and the vertical difference between the end points is 13.48 m, the track irregularities were not taken into account for this work.



Figure 51. Satellite view of the portion of the track investigated in the model (Google maps).

The profiles of the rails and the wheels were a result of an optimization analysis performed by the National Research Council NRC [10], the wheel profile is known as NRC-MM but for this work a new ORE S1002 was used. Worn profiles were used for the inner and outer rail, the rail profiles are CPC and HRC respectively, all the profiles were measured using a MiniProf Rail instrument; Figure 52 shows the profiles and the corresponding contact areas calculated from the multibody simulation.

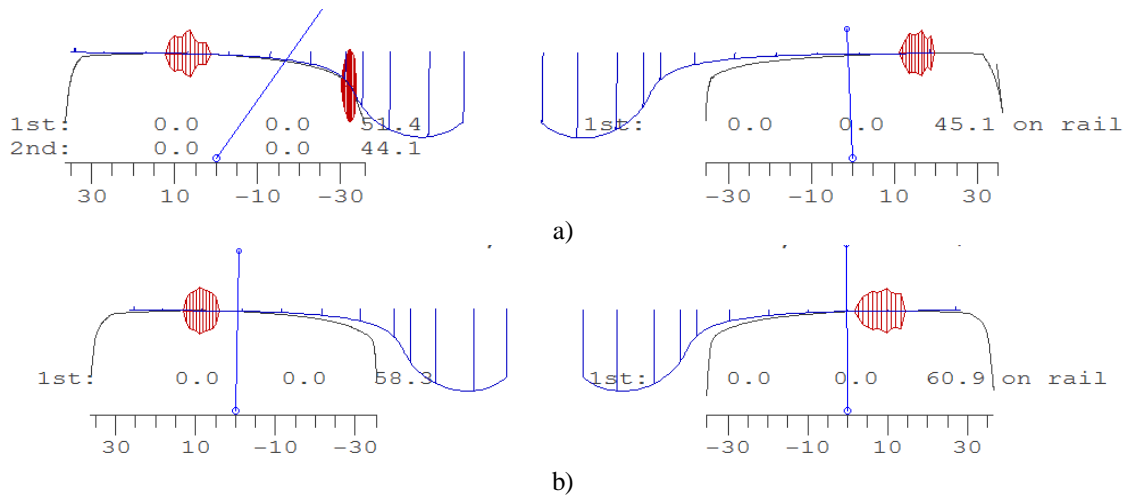


Figure 52. Measured worn rail and s1002 wheel profiles and their respective contact areas, a) In the curve 4 b) On straight track

5.5 Energy and wear calculations

5.5.1 The wheel/rail contact problem

During the multibody simulation of the vehicle passing the curve, a contact module evaluates the contact forces, which are needed in the dynamic equations of the wheelsets. In this study a multi-Hertzian-Fastsim approach is employed for this purpose.

In the first step the exact position of the wheelset is used to determine the interpenetration regions between the wheel and the rail, considering both wheel and rail as rigid objects. In each interpenetration region (up to three per wheel/rail pair) Hertzian theory is used to obtain a normal contact force and a contact pressure distribution based on the penetration between wheel and rail and the local curvature of the contacting bodies.

The second step is to evaluate the tangential contact forces. To such end the simplified theory of Kalker [6,7] is used. This assumes that the tangential stress in the contact area is proportional to the tangential displacement and limited by Coulomb's law. The details of this theory as well as a *Fortran* code of the implementation, Fastsim, are given in [6]. In multibody analysis the moment around the normal of the contact point is normally neglected as it has only a very small influence on the wheelset's dynamics. However, for the frictional energy considered in this study this moment is relevant, therefore Fastsim has been modified so that this moment is also calculated.

5.5.2 Energy calculations

The local energy (per unit of volume) dissipated at a point of the contact area is the scalar product of the local slip and the local tangential stress, so the total energy dissipated in the whole contact patch is equal to the surface integral of the local energy. Accordingly, the



power dissipated as a consequence of frictional work is often approximated by ignoring the contribution of the spin as:

$$P_{frict} = (T_x\gamma_x + T_y\gamma_y)V \quad (19)$$

Where V is the velocity of the vehicle, T the tangential force, and γ the creepage (normalized slip). When the contribution of spin is included it becomes:

$$P_{frict} = (T_x\gamma_x + T_y\gamma_y + M\varphi)V \quad (20)$$

Where M is the spin moment and φ is the spin creepage.

The methods described in equations (19) and (20) are compared, so that the consequence of neglecting the spin contribution can be quantified.

5.5.3 Wear calculations

The Derby wear index used by Pearce and Sherratt, mentioned in section 3.1.5, is proposed to calculate the wear rates at a specific point of the track since it adopts an energy concept in the analysis of the relationship between wear rate and contact conditions, where the wear rate (expressed in $\mu\text{g}/(\text{m mm}^2)$) is related to frictional work done at the wheel–rail contact as:

$$Wear_{Rate} = KT\gamma/A \quad (21)$$

Where, K is a wear coefficient and A is the contact area.

The wear rate represents the mass of removed material per unit distance traveled by the vehicle (expressed in m) and per unit surface (expressed in mm^2).

In order to determine the wear coefficient K , correlations performed by F. Braham et al. for the wear model between the wear rates and the wear index in each regimen are used (see Figure 14). The wear coefficient is defined for each of these regions as the equation (22) shows [28]:

$$Wear_{Rate} = \begin{cases} 5.3I_w & I_w < 10.4 \\ 55.0 & 10.4 \leq I_w \leq 77.2 \\ 61.9I_w & I_w > 77.2 \end{cases} \quad (22)$$

Where I_w is the wear index.



RESULTS AND DISCUSION

6.1 Friction coefficient measurement in the field

In order to determine the friction coefficient under dry condition, measurements using the hand-pushed tribometer FR 101 were performed previously to the installation of the Hy-Power lubrication system. The dry friction coefficient sets a reference measure to compare with the other conditions. Subsequently, the Hy-Power lubrication system started to operate and the friction coefficient decreased about 33.9%.

Several track visits and friction coefficient measurements were carried out to determine the effective lubrication distance using HLK. Figure 53 shows the lubrication condition in different position over the track, where BT and ET relate to the beginning and the end of the transition, respectively. The green-framed insert shows a portion of the rail where the HKL is not present anymore, in which the zone 2 shows the rolling band without lubricant followed by the oxide band, zone 1. According to the measurements, the effective lubrication distance is approximately 210 meters, meaning that the lubrication conditions set in the Hy-Power controlled device are not adequate to carry the grease to the entire curve.

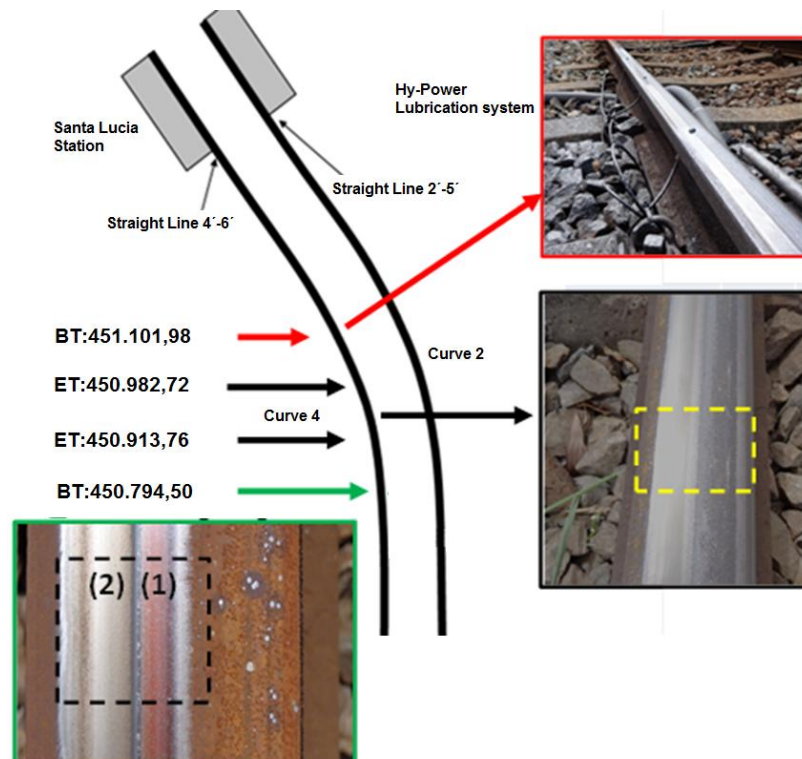


Figure 53. Effective lubrication distance using HLK. The left Figure (in green) shows zone 2: the rolling band without lubricant and zone 1: the oxide band. The right top figure (in red) is the position where the lubrication system Hy-Power is installed and the right bottom figure (in black/yellow) is the middle of the track.



When the supply of HLK ends, friction measurements are performed to establish the friction coefficient value under Post-HLK conditions. This condition produces a remnant layer on the track and the friction coefficient increases about 15.9% regarding to the HLK condition but it is still lower than the dry condition.

Figure 54 shows the different values obtained from the friction measurements in curve 4 under the three different lubrication conditions. HLK reached a value close to the optimal friction coefficient proposed by [2], 0.35, and it starts to increase when the layer of lubricant became thinner in the Post-HLK condition. These friction coefficients were implemented in the multibody model to perform the dynamics analysis.

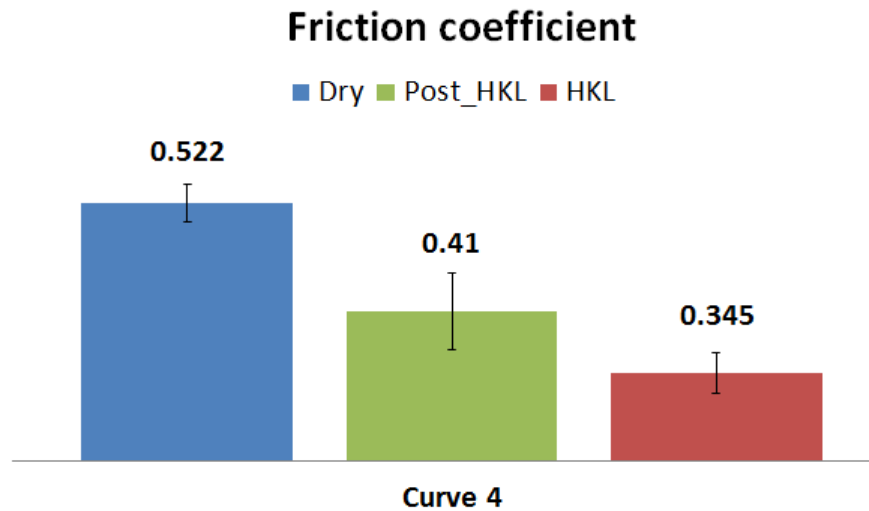


Figure 54. Average friction coefficients measured in curve 4.

6.2 Power consumption measurement in the field

Figure 55 to Figure 57 show the results of the energy consumption measurement under each lubrication condition and the corresponding velocity profiles. The measurements were performed twice under similar conditions. The inertia variations in the vehicle (acceleration) have a significant role on the energy consumption; therefore it is only possible to compare the measurements with similar velocity profiles. According to that, Figure 58 shows the results of the energy consumption measurements under the three contact conditions with the most similar velocity profiles, only these data were processed and analyzed to be compared with the simulation results.

The remaining power related to the contact dissipated energy is calculated according to equation (17). Table 4 shows the energy consumption for each friction condition, as well as the reduction in energy consumption compared with the reference dry condition. As it was mentioned before, the kinetic energy is the dominant component in the energy consumption as it is equivalent to circa 73.9% of the total energy, while the potential and drag energy are equal to 9.3% and 3.4% respectively. Hence, the energy dissipated in the wheel-rail contact accounts for 13.5% of the total energy consumption.



The results in Table 4 show a power saving of 15.3% in the wheel-rail contact after using HLK and 9.4% in the post-HLK condition.

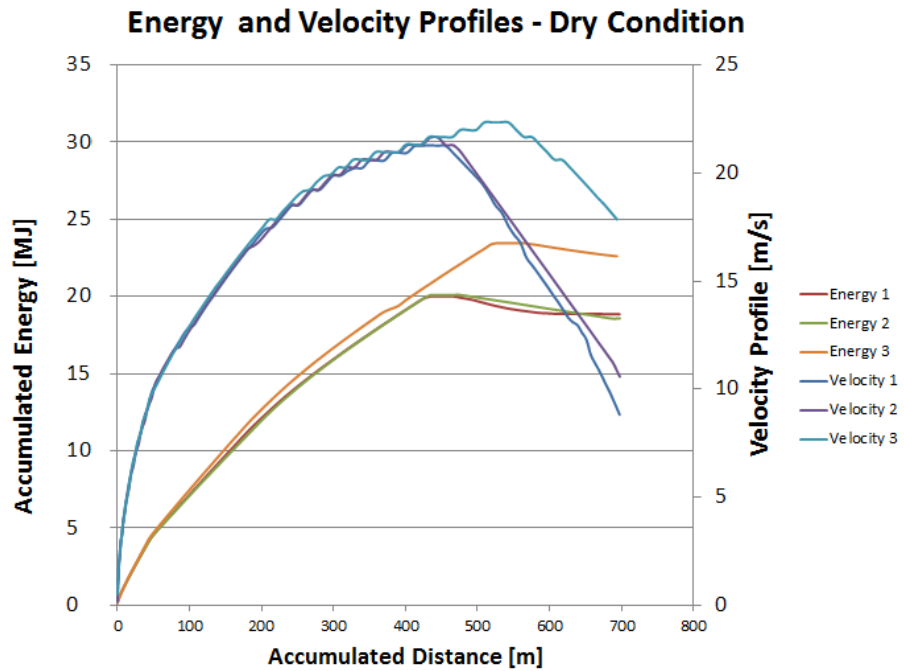


Figure 55. Accumulated energy and velocity profile under dry condition.

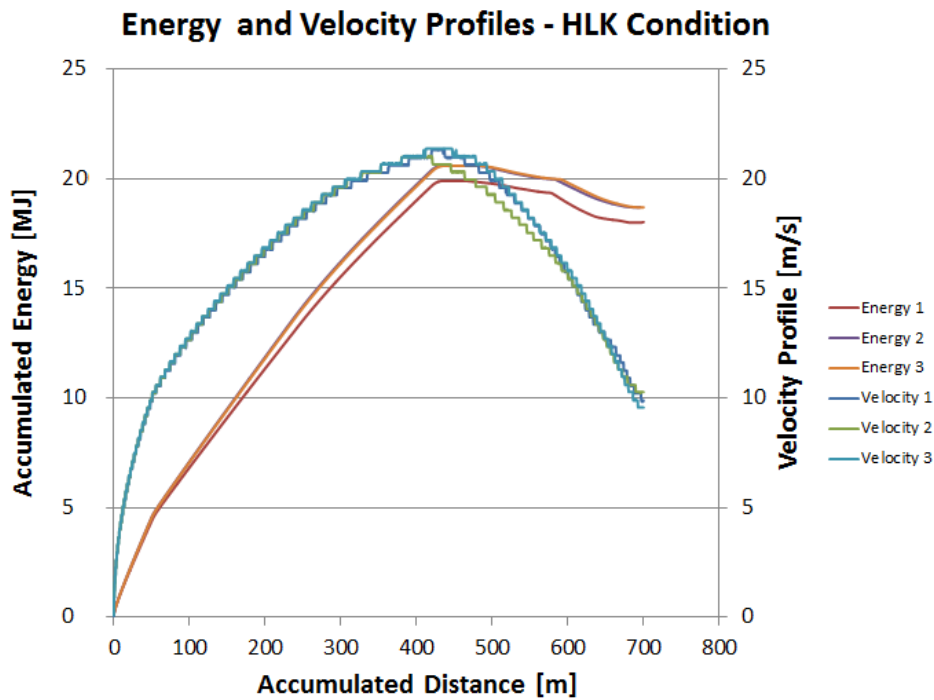


Figure 56. Accumulated energy and velocity profile under HLK condition.

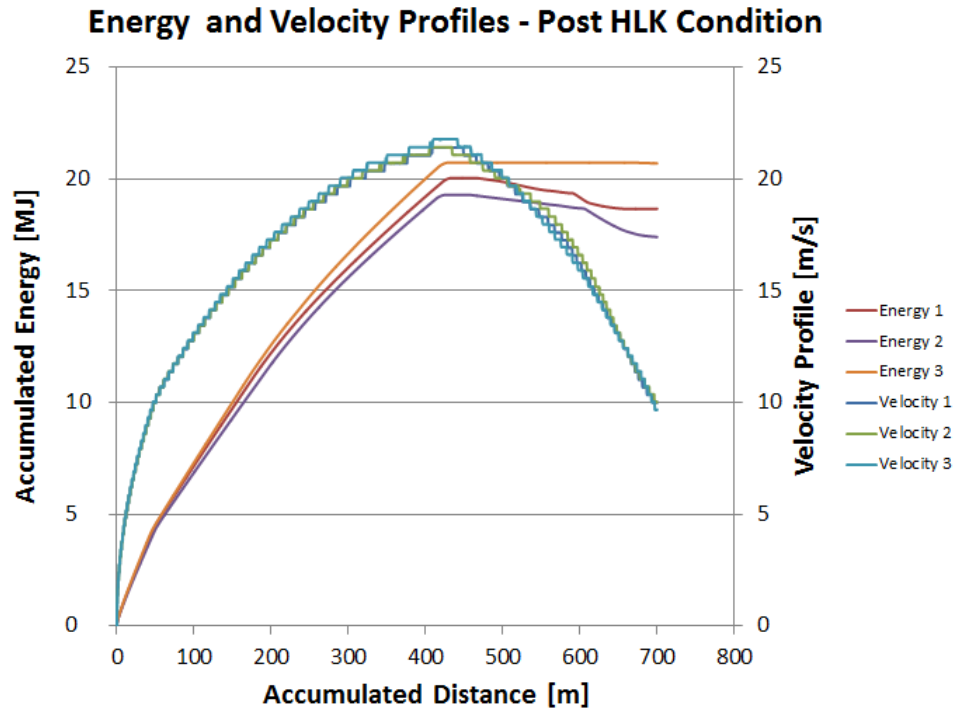


Figure 57. Accumulated energy and velocity profile under post HLK condition.

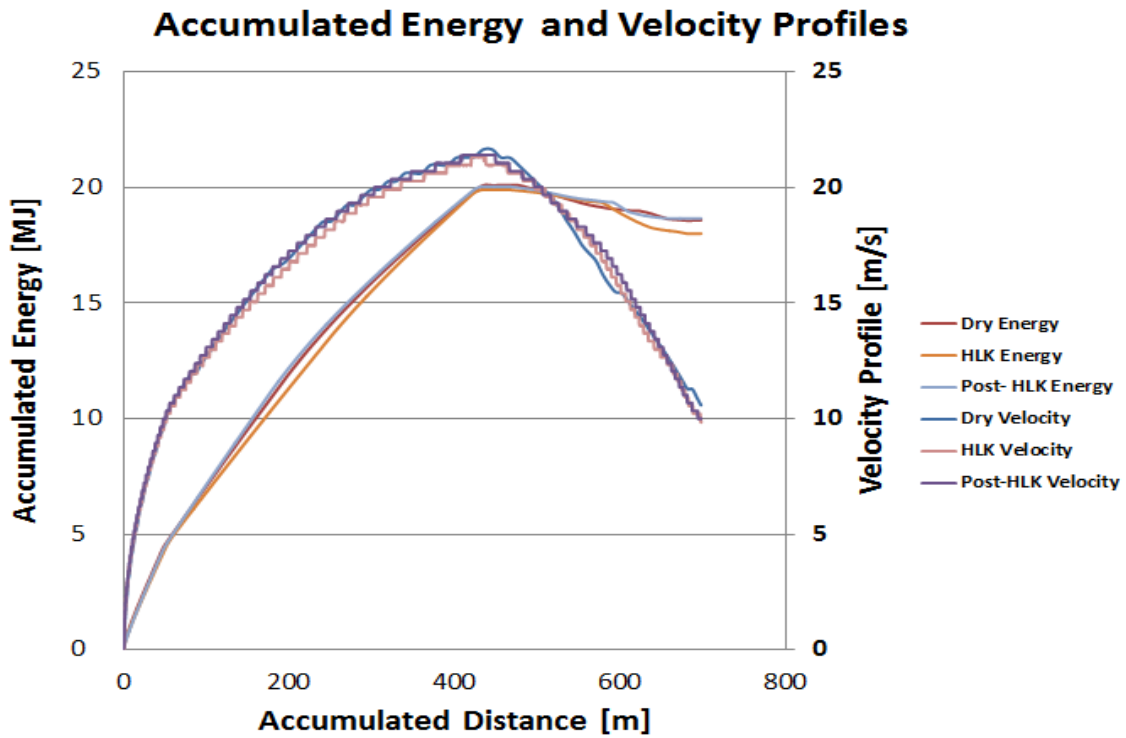


Figure 58. Energy and velocity comparison between the three lubrication conditions.



Table 4. Reduction in energy consumption due to application of a friction modifier on the rail.

	Dry [KW]	Post_HLK [KW]	HLK [KW]
P_{tot}	812.57	799.99	793.51
P_{kin}	606.17	584.64	585.66
P_{pot}	60.76	81.04	82.00
P_{drag}	27.99	27.66	26.17
P_{rest}	117.66	106.65	99.68
% Reduction	-	9.4%	15.3%

6.3 Calculation of the moment of force of a Wheel

Figure 59 shows the equation of the vehicle velocity under dry condition, the tendency curve is described by a 6th grade polynomial, which is derived in order to get the acceleration equation for the moment of force. Once the acceleration equation is calculated, the moment of force is obtained using the equation 18, which is applied to each wheel using a force actuator in VI-Rail Adams. Figure 60 and Figure 61 show the torque generated in a wheel and the velocity curve of the vehicle model calculated from the multibody simulation.

It is possible to see that the velocity curve of the vehicle from the field data is similar to the vehicle model curve from Adams (see Figure 59 and Figure 61), meaning that the calculation vehicle model displacement over the track is in very good agreement with the field measurements.

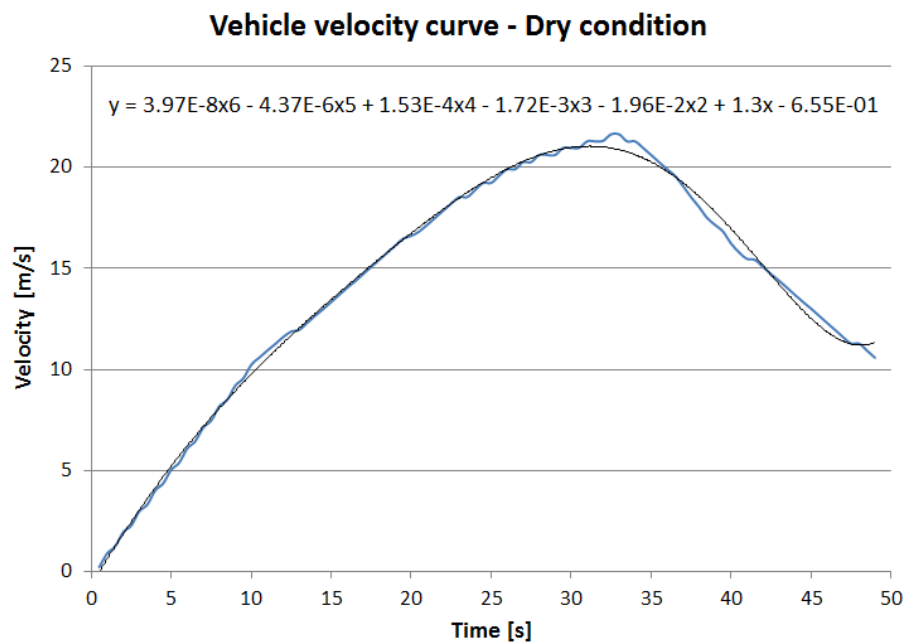


Figure 59. Vehicle velocity curve calculated from field measurements.

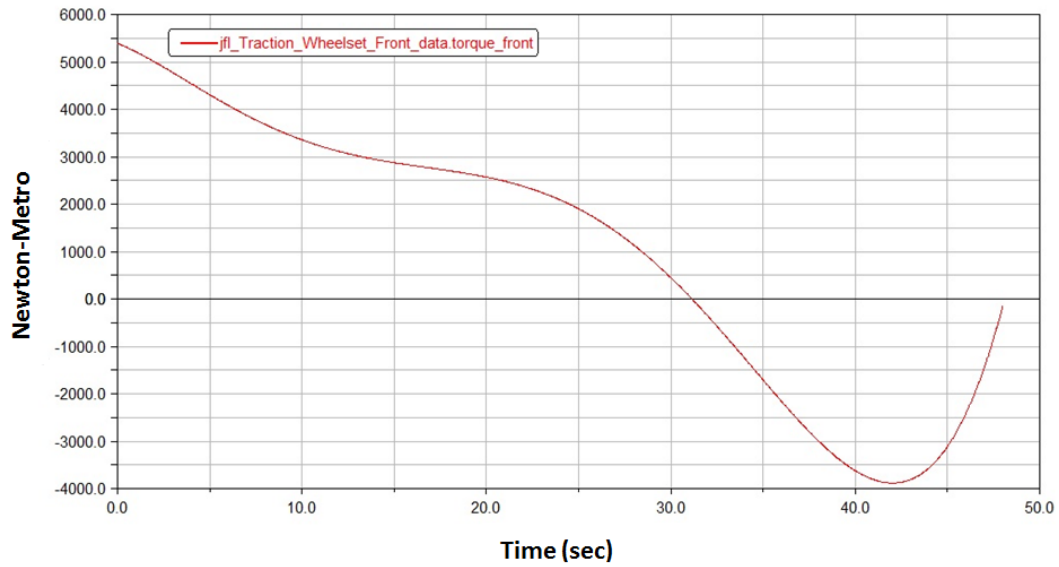


Figure 60. Traction moment applied to each wheel of the leading and the trailing vehicle in the vehicle simulation

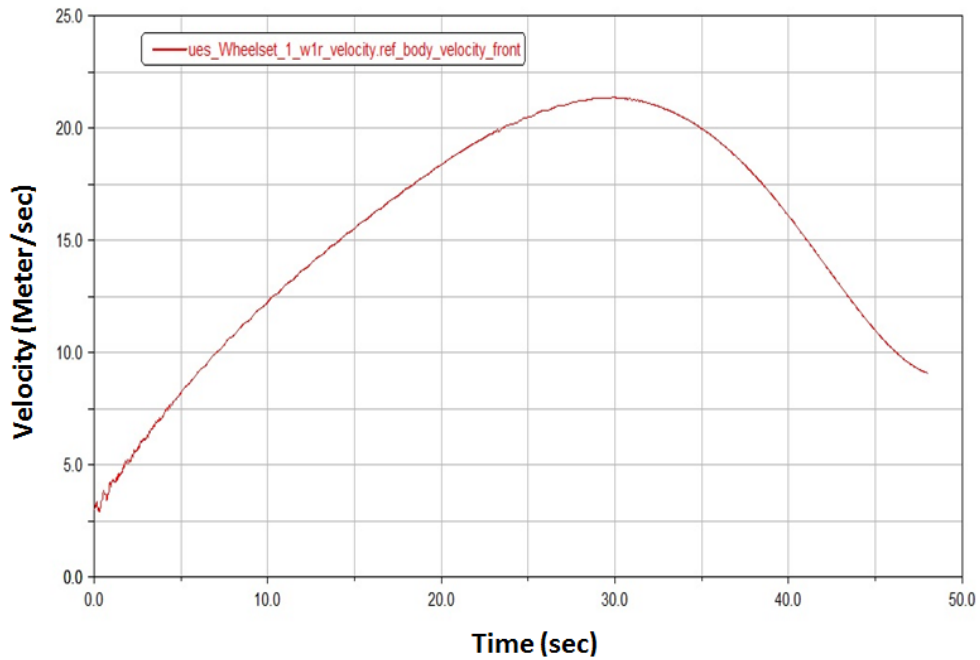


Figure 61. Velocity curve of the vehicle model calculated from the multibody simulation.



6.4 Power and wear calculations

Several simulations were performed under the three friction conditions in order to compare the calculated energy consumption in the contact with the field measurements. Also, the results of wear calculations using the equation 21 are presented.

The study was divided in two parts. The first one was related to the calculations of energy consumption in the contact and wear rate of the whole vehicle, which was performed without traction, and the second part was only done on the first bogie but taking into account the traction on the wheels.

It is worth to mention that all energy savings calculated in this section are related with energy dissipation in the contact interface, which represents around 13.5% of the total energy consumption.

6.4.1 Power calculations

Table 5 shows the accumulated energy consumption in the wheel/rail contact for all the wheels of the vehicle. The calculation is performed using Equation 20 with basis on the output of the vehicle simulation.

From the field measurements it was found that there is a power saving of 15.3% using HLK and 9.35% in the post-HLK condition, while the energy calculations using multibody simulation show 35.6% and 21% respectively.

Table 5. Energy simulation results.

	Total Power [KW]	% Reduction
Dry	106.73	-
Post_HLK	84,28	21.0%
HLK	68.74	35.6%

The distribution of the total energy dissipated in the contact is presented in the Table 6 and Figure 62 shows how this total energy is distributed in each wheel. The outer wheels consume 86.1% of the total energy and the 71.1% of this energy is dissipated in longitudinal friction work. This behavior is due to the fact that the outer wheel has a higher rolling radius than the inner wheel as Figure 52a shows. This condition generates a high longitudinal velocity in the contact, increasing the longitudinal creepages and creep forces.

On the other hand, the inner wheels consume 13.9% of the total energy and 66.6% of this energy is dissipated in lateral frictional work. Unlike the outer wheels the longitudinal creep forces and creepage are not significant and the high energy consumption takes place in the lateral direction.



The contribution of wheel/rail spin to the energy consumption is of circa 7% and under dry condition this is 7.47 kW. It is worth noticing that although the relative percentages associated to spin dissipation power for outer and inner wheels are similar in Figure 62, they represent quite different power magnitudes since the total energy consumption of outer wheels is about six times higher than that of inner wheels.

Table 6. Total energy distribution.

Outer Wheels	86.1%	Longitudinal	64.5%
Inner Wheels	13.9%	Lateral	27.4%
		Spin	8%

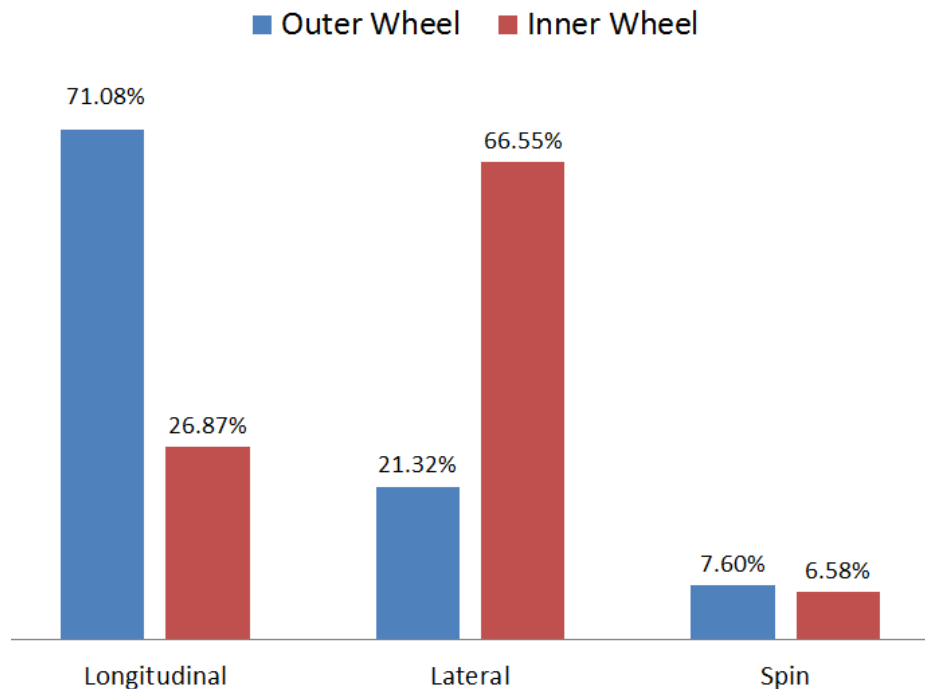


Figure 62. Contribution of the energy consumption of lateral, longitudinal and spin per wheel.

Figure 63 shows the power consumption per bogie. The first bogie of each coach has higher consumption. This happens because the first bogie guides the vehicle through the curve, while the rear bogie just follows [60]. Moreover, it was possible to identify from the data that the first wheelset of each bogie consumes in average 72.5% more energy than the second one.

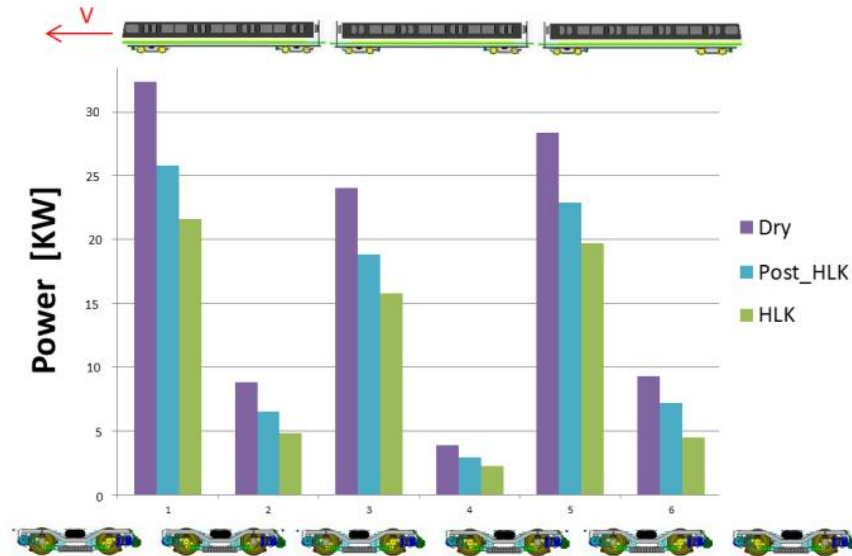


Figure 63. Simulated energy consumption per bogie.

A linear correlation between the power consumption and the friction coefficient is presented in Figure 64 for the three friction conditions, the slope of the energy calculations using multibody simulation is twice the value found in the field measurements.

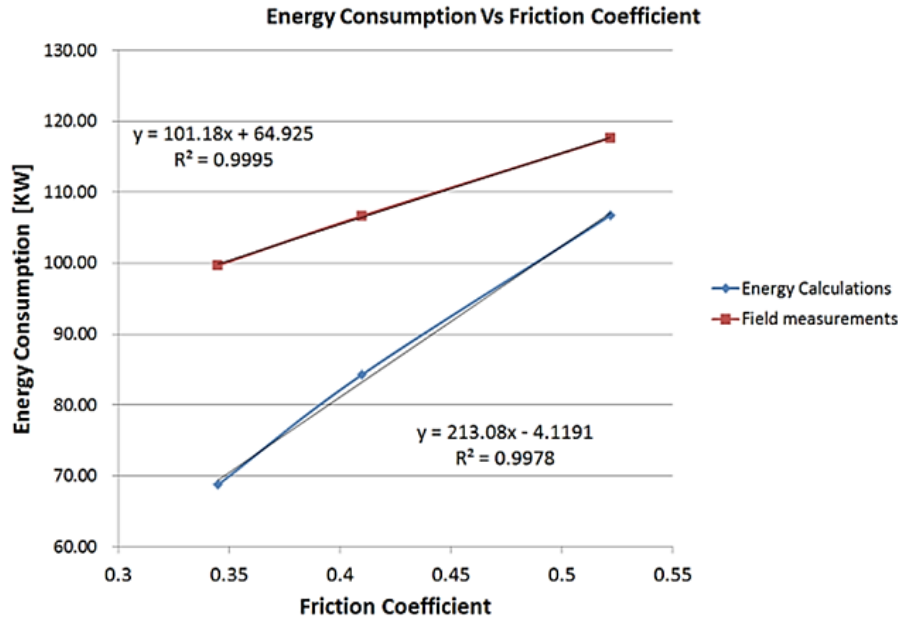


Figure 64. Linear correlation between power consumption and Friction coefficient in both simulations and field measurements.

In order to identify the effect of the friction coefficient in the energy dissipation in the wheel-rail contact, several simulations were performed varying the friction coefficient from 0.2 to 0.7. Figure 65 and Figure 66 show the results of the total energy consumption



under different friction coefficients for the inner and outer wheels of the first bogie of the vehicle. The results were obtained using the Tgamma method and Fastsim, the latter allows determining the behavior of the spin energy dissipation since the Tgamma does not take into account this component. So the energy dissipated in spin is the difference between the two curves.

Figure 65 shows that the inner wheels energy consumption rises as the friction coefficient increases. However at a friction coefficient near to 0.4, the energy consumption starts to decrease. For the outer wheels this behavior is not present and the energy consumption continuously increases with the friction coefficient, see Figure 66. When the Fastsim and Tgamma results are compared it is possible to see that the energy dissipation generated by spin increase with the friction coefficient in both inner and outer wheels.

The energy dissipation in the outer wheels is around ten times higher than the inner wheels energy.

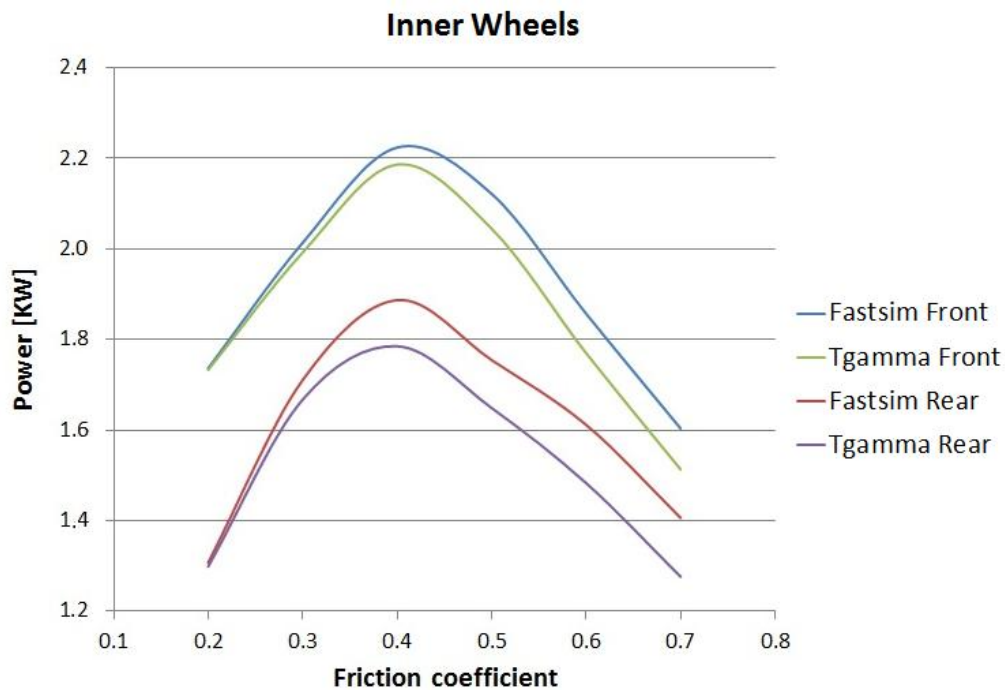


Figure 65. Effect of the friction coefficient in the total energy dissipation for the inner wheels.

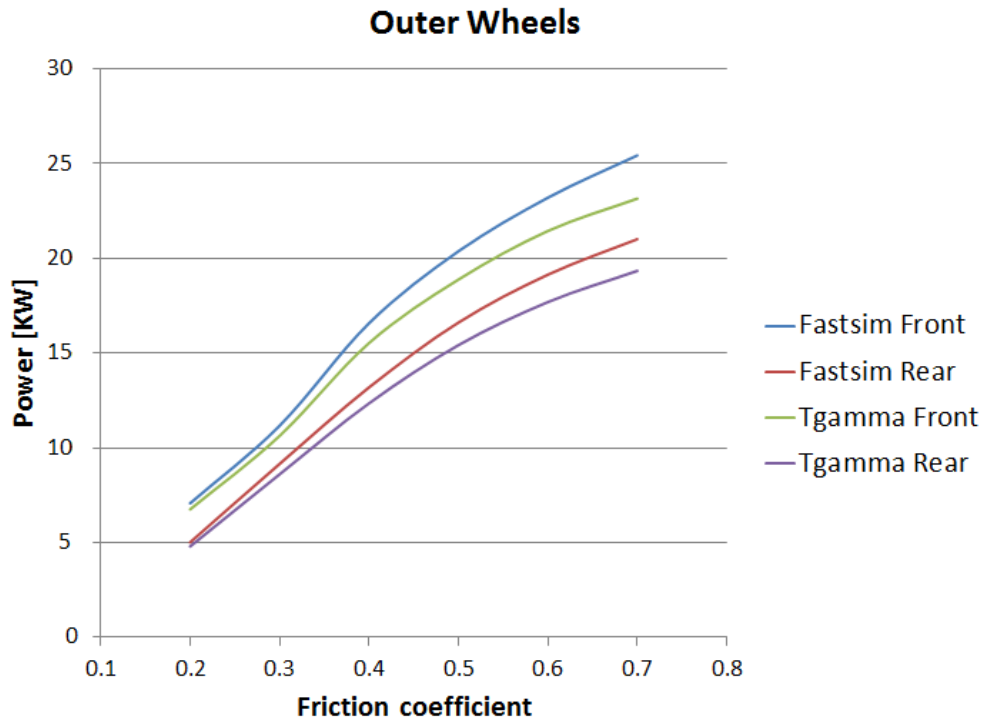


Figure 66. Effect of the friction coefficient in the total energy dissipation for the outer wheels.

With the aim of explaining the behavior seen in the previous results, Figure 67 shows the energy consumption in the longitudinal and lateral direction and Figure 68 shows the creepage and creep force for the inner and outer wheels. From Figure 67c and Figure 67d, it is possible to see that both the inner and outer wheels show the same behavior for the lateral energy dissipation. In other words, the lateral energy consumption goes up until a friction coefficient between 0.4 and 0.5 is reached and then goes down. However, for the outer wheels the longitudinal energy is much more significant than the lateral component, then, so when the total energy is calculated in Figure 66, it is not influenced by the lateral behavior. On the other hand, in inner wheels the lateral energy dissipation is more significant and the longitudinal component decreases as the friction coefficient grows. Hence, the behavior of the lateral component dominates in the total energy calculation for the inner wheels as Figure 65 shows.

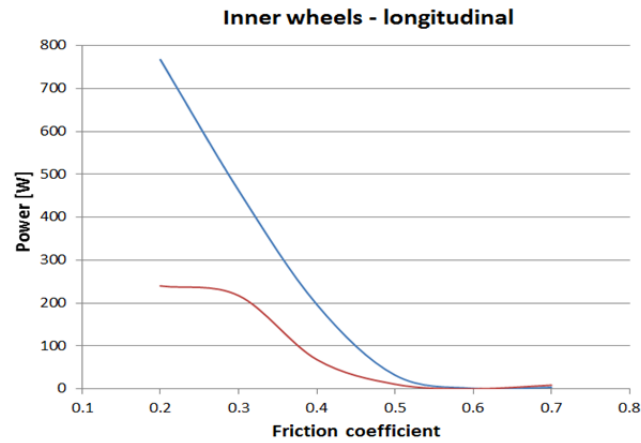
Figure 68b shows the longitudinal force present in the inner and outer wheels. It can be seen that at a friction coefficient of 0.2 both wheels have a similar longitudinal creep force. As the friction coefficient increases, however, the inner wheel loses traction while the outer wheel increases it, keeping the total traction constant. These results explain the behavior of the energy consumption shown in Figure 67a and Figure 67b, where the energy dissipation decreases in the longitudinal direction for the inner wheel and increases for the



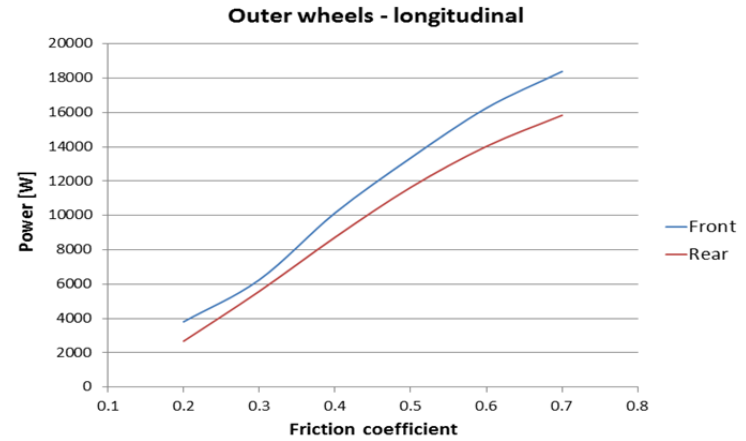
outer wheel. Although the longitudinal creepage decreases in both inner and outer wheels (see Figure 68a), it is not dominant for the outer wheel.

The lateral creepage for the inner and outer wheels is shown in Figure 68c. It decreases linearly as the friction coefficient grows. This behavior is explained because the difference in the longitudinal creep force for the inner and outer wheels produces a rotational moment of the wheelset in clockwise direction, reducing the yaw angle of the wheelset. On the other hand the lateral creep forces, shown in Figure 68d for the inner and outer wheels, increase as the friction coefficient grows, however after a friction coefficient of 0.4 the creep force tends to stabilize, this condition produces that the energy consumption reaches a peak and later starts to decrease, as Figure 68c and Figure 68d show.

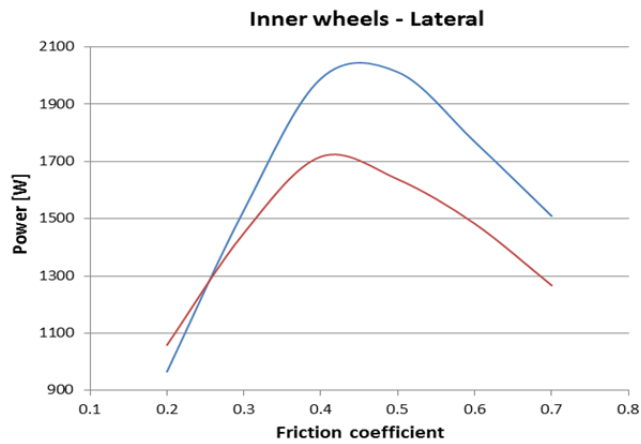
Figure 69 shows the total energy consumption of the first bogie, where the outer wheels provide 89.8% of the total energy dissipated. According to these results, it is possible to conclude that the total energy consumption increases linearly as the friction coefficient grows.



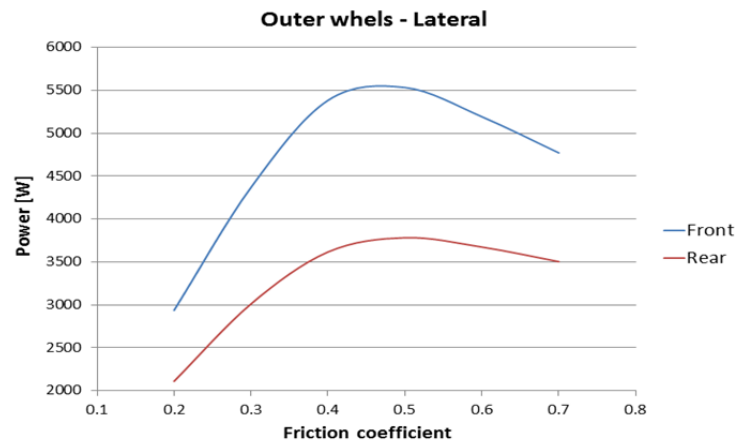
a)



b)



c)



d)

Figure 67. Power consumption of the inner and outer wheels in longitudinal and lateral direction.

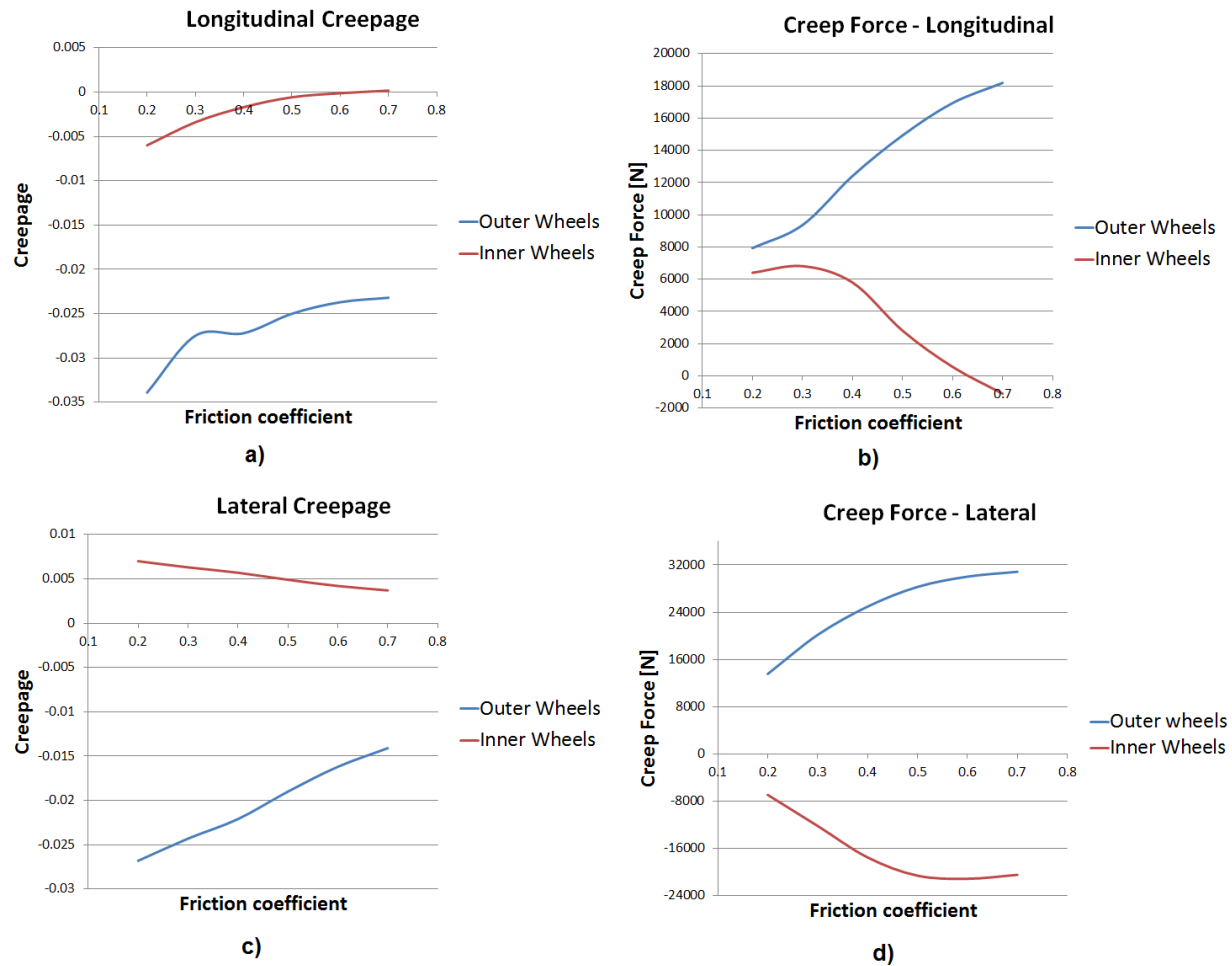


Figure 68. Creepages and creep forces in longitudinal and lateral direction.

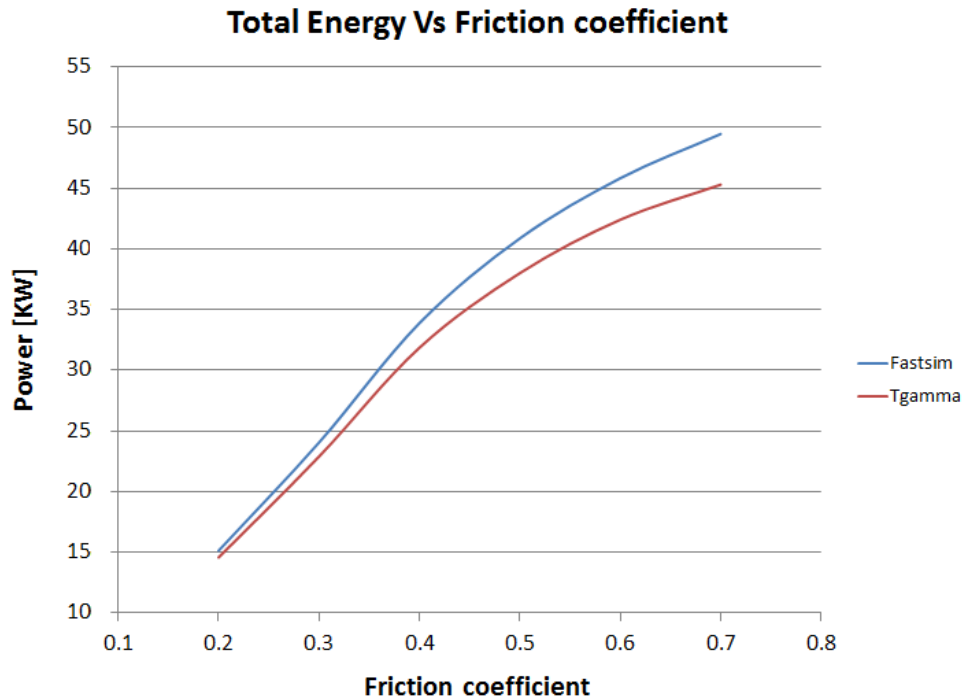


Figure 69. Total energy consumption of the first bogie.

6.4.2 Wear calculations

The data obtained from the simulation were used in order to calculate the wear rates of the wheels using the equation 21 and 22. Figure 70 shows the accumulated wear rates per wheel side without taking into account the traction. As it was expected, the outer wheels have the highest wear rate since the wear is related with the energy dissipation in the contact by means of the friction work.

Figure 70 shows that the highest wear rate takes place under dry condition and it decreases when the friction modifier is applied; this condition is present only in outer wheels. As a matter of fact, the wear rate is 19.8% and 36.1% lower under Post-HLK and HLK condition, respectively. This means that, according to the calculations, the wheel lifetime can increase at least in 20% when a friction modifier is used. However, when the wear rates of the inner wheels are analyzed it is concluded that the benefits for the lifetime of the inner wheels are rather limited.

Figure 71 and Figure 72 show the wear rates for the inner and outer wheel in longitudinal and lateral direction as function of the friction coefficient, which were calculated for the first bogie of the vehicle. The behavior of the wear results is similar to that found in the energy consumption results.



Figure 70. Accumulated Wear rate per wheel side for the entire vehicle.



Figure 71. Effect of the fiction coefficient in wear rates of the inner wheels of the first bogie.

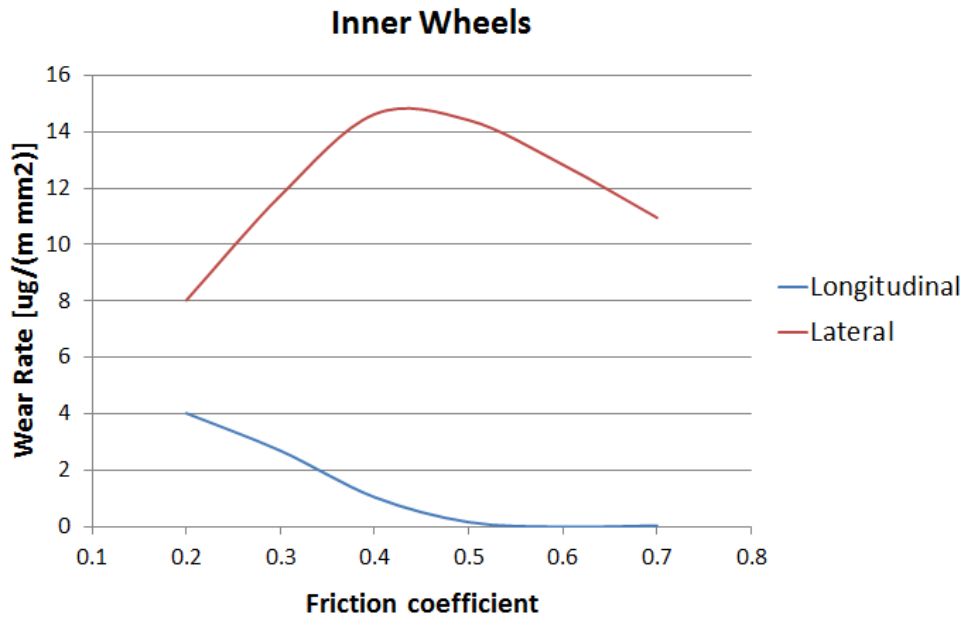


Figure 72. Effect of the fiction coefficient on the wear rates of the outer wheels of the first bogie.

6.4.3 Profiles effect in the energy consumption and wear rates

The quality and type of profiles play an important role in the energy consumption and wear rates. When the profiles are not designed to work together or when the profiles are worn the contact is similar to Figure 52a. It is possible to see that the outer wheel has two patches of contact with different rolling radii; therefore the longitudinal creepage in the contact patches is also very different (see equation (4) of section 3.2). According to that, it is not possible that both of the contact patches roll with a radius that is perfect for curving (creates the rolling radius difference with the contact patch at the other wheel that corresponds to the curve radius), or that the creepage is optimal for to create the required longitudinal creep force (traction). At least one of the contact patches and probably both are rolling in a non-optimal rolling radius. This gives rise to a high energy consumption at the wheels with two point contact. A way of looking at this is that the difference in the rolling radius and subsequently in creepage and creep force, creates an unwanted moment, as the longitudinal force is the only frictional force/moment that is desired (for acceleration). This moment gives rise to energy losses. On other hand when the profiles are designed ideally and they are new, a single contact path is present in the outer wheel as Figure 73 shows.

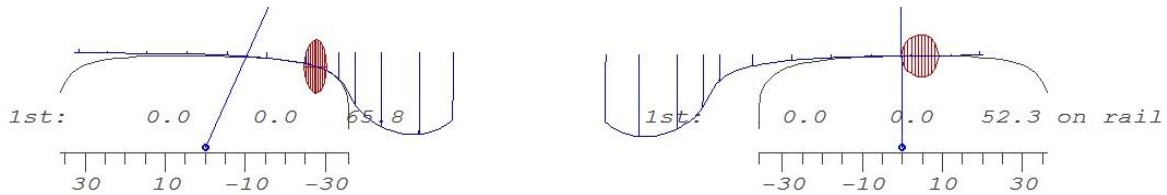


Figure 73. Optimal wheel and rail profiles (new UIC 60 and New Ore S1002).

As Table 7 shows, two couples of rail and wheel profiles were studied in order to know the effect of the profiles quality in the energy consumption and wear rates. The measured profiles are composed by the Metro of Medellin rail profiles (CPC and HRC, inner and outer rail respectively) and a new Ore S1002 profile for the wheels, these profiles are not designed optimally to work together and the contact patches are shown in Figure 52a. While, the standard profiles are composed by a new UIC 60 and New Ore S1002 for the rail and the wheel respectively, which are designed to work optimally and their contact patches are shown in Figure 73.

Table 7. Measured profiles and standard profiles

Couple	Rail profiles	Wheel profiles	Designation
1	Worm CPC-HRC	New Ore S1002	Measured Profiles
2	New UIC 60	New Ore S1002	Standard Profiles

Simulations and energy calculation were performed using the profiles presented by the Table 7 under a friction coefficient of 0.4, Figure 74 shows the comparative results between measured profiles and standard profiles. As it was mentioned previously, Figure 74a shows an increment in the longitudinal creepage of the outer wheels due to the double contact patch, as well as, an increment in the lateral creepage, meaning that the wheelset has a lower yaw angle using the standard profiles, which improve the vehicle navigation over the curve.

Figure 74b, Figure 74c and Figure 74d show the results in the total energy consumption of the first bogie. It can be observed energy savings of 68.6%, 81.08 and 61% in the longitudinal, lateral and spin direction when optimal profiles are used. This is more influential than the friction modifiers, which only reach a maximum energy saving of 35.6% according to Table 5.

Figure 75 shows the differences between measured profiles and standard profiles regarding to the wear rates. An increase of 80.7% is possible using new optimal profiles, which is 2 times higher compared to the friction modifier reduction.

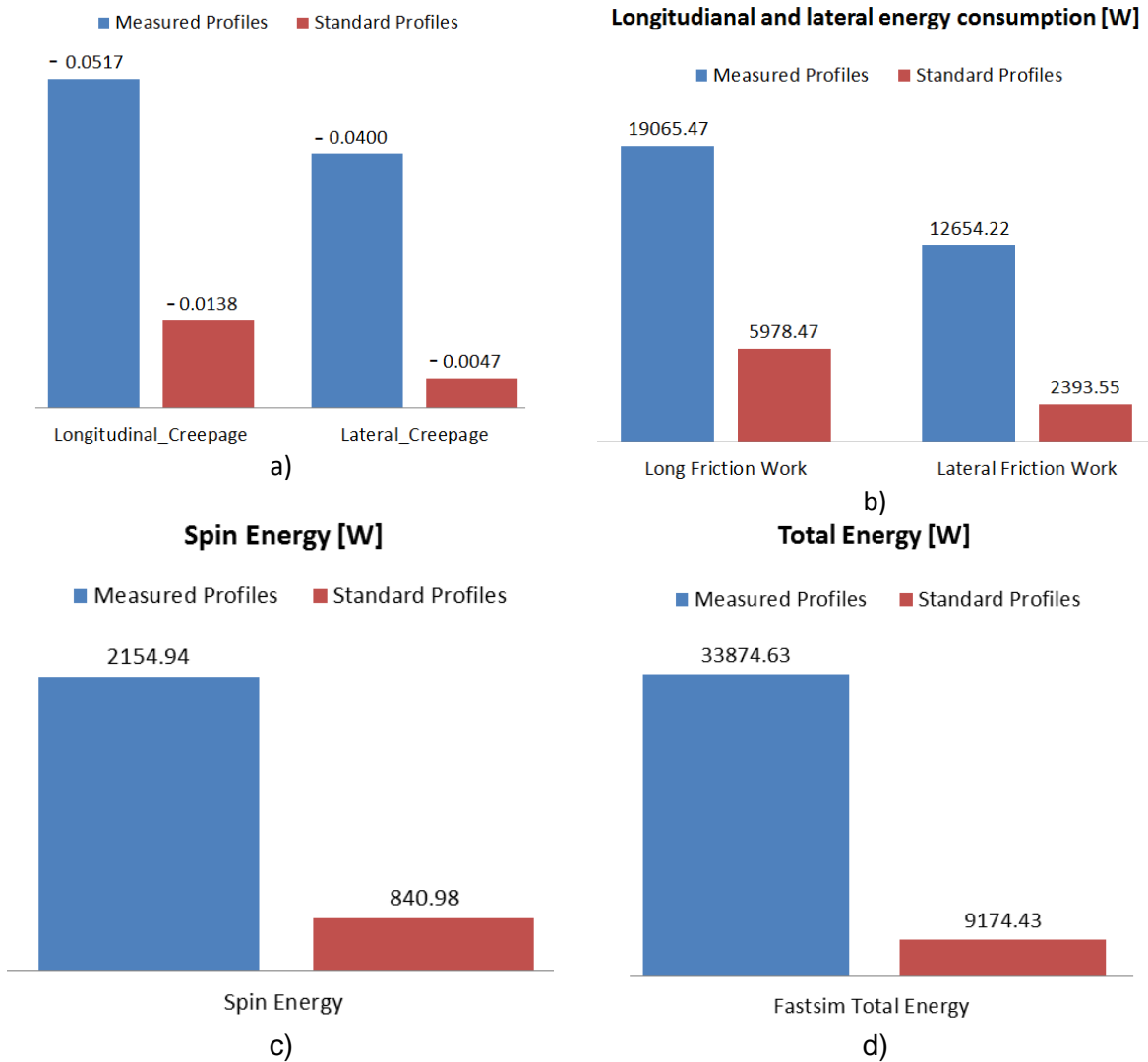


Figure 74. Effect of the measured profiles and standard profiles in the energy consumption and creepage. a) Longitudinal and lateral creepage in the outer wheels, b) Longitudinal and lateral energy dissipation in all the wheels of the first bogie, c) spin energy dissipation, d) total energy consumption of the first bogie.

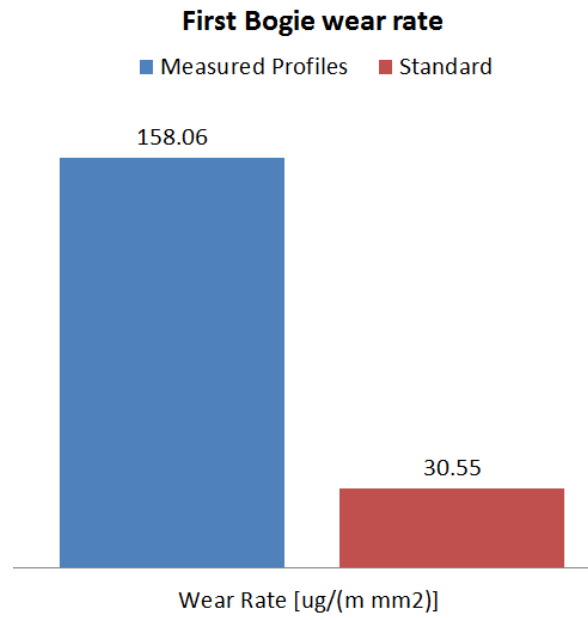


Figure 75. Wheel/rail profiles effect in the wear rates of the first bogie.



CONCLUSIONS AND RECOMMENDATIONS

- The lubrication system Hy-Power was not able to carry the friction modifier HLK to the entire curve 4 under the 2X3 configuration (Two pumping pulses every three vehicles). It is important to change the parameters of the Hy-Power control device in future, in order to reach the whole curve. Also a rain sensor should be installed to stop the system in rainy weather to prevent wheel slip condition when braking.
- The vehicle model, including traction, using VI-Rail ADAMS, reproduces the measured velocity curve of the real vehicle. This allowed obtaining results similar to what is observed in the field in terms of some variables such as acceleration, position, forces and contact parameters.
- Despite of a difference near to 56.3% between the field energy measurement and the simulation results, both methodologies result in the same trend: the energy consumption reduces when the friction coefficient decreases. This allows studying the influence of the contact conditions on the energy dissipation and wear rate.
- The change in the kinetic energy of the vehicle represents the highest energy consumption in the vehicle, while the energy dissipated in the wheel-rail contact is less than 13.5% of the total energy consumption. However, due to the high operational costs, a small reduction in the energy contact dissipation potentially means big savings for the company.
- Using a friction modifier, such as HLK, can result in a reduction of at least 9.3% in energy consumption in the contact and 19% in the wheel wear rate. This means a saving near to 1.2% in the total energy.
- Only for low friction coefficient conditions it is recommended to neglect the effect of the spin moment in the energy calculations, since under dry condition it represents 6.61% of the energy consumed at the contact (7.83 kW).
- The friction coefficient has strong influence on the energy consumption and wear rate of the outer wheels. More energy is saved when the lowest friction coefficient is applied. However, it should always be assured that there is enough friction for the required traction and braking.
- Since the friction modifier does not have a significant effect on the energy consumption and the wear rates of the inner wheels, it is not recommended to lubricate the inner rail, Following this recommendation would allow saving grease as well as, installation and maintenance costs of the lubrication system.
- The energy consumption can also be employed to monitor the lubrication condition of wheel/rail contact, to facilitate maintenance of lubrication systems.



- The results of simulations with different profiles are very important since they show the necessity for optimizing profiles and re-profiling procedures. An optimized wheel-rail profile combination greatly reduces the energy dissipation and the wear rates. This reduction is estimated to be twice the reduction achieved by the friction modifier.
- For future work it is recommended:
 - To study the difference between measured and calculated energy consumption
 - To perform a further analysis of the spin energy dissipation using WEAR method proposed by [14] and [48].
 - To carry out a study to identify the wheel profile when the double contact take place in the outer wheels and how long it takes for a new wheel profile to get to this state.



REFERENCES

- [1] J.F Santa. Development of lubrication system for wear and friction control in wheel/rail interfaces. Doctoral thesis, National University of Colombia. (2012)
- [2] Transit/high speed mounted on board transit/high speed rail gauge face lubrication system.
Available online: <http://www.kelsan.com/solutions/solutions.html>
- [3] R. Larke, Survey of wheel/rail lubrication practices. Engineering Research Programme. Report No. ITLR-T12442-001.7 (2003)
- [4] V. Reddy, G. Chattopadhyaya, P. Larsson-Kråkb, D. Hargreaves. Modelling and analysis of rail maintenance cost. *Int. J. Production Economics* 105 (2007) 475–482.
- [5] H. Grausse, G. Poll. Wear of wheel-rail surfaces. *Wear* 113 103-122 (1986)
- [6] J. Kalker. A Fast Algorithm for the Simplified Theory of Rolling Contact, *Vehicle System Dynamics* 11 (1982), pp. 1–13.
- [7] K. E. Zaaza and A. L. Schwab, Review of Joost Kalker's wheel-rail contact theories and their implementation in multibody codes. IDETTC/CIE 2009, 9, San Diego, California, USA.
- [8] G. Idárraga, J. Sánchez, J.F. Santa, A. Toro. Identificación de mecanismos de desgaste en rieles de vía comercial del metro de Medellín. *Revista Colombiana de Materiales* N. 5 pp. 72-77 (2013).
- [9] L. Grassie, J. Kalousek and E. Magel. Treatment of Rail Corrugation and Problems of Wheel and Rail Damage, National Research Council, Internal Report Metro of Medellin, (1999).
- [10] J.F Santa, J.C Sánchez, M. Palacio, R. Toro, A. Toro. Wear assessment in a commercial railroad: correlations between rail wear rates and operating conditions. 9th International Conference on Contact Mechanics and Wear of Rail/Wheel Systems (CM2012), Chengdu, China, August 27-30 (2012).
- [11] P.A. Cuervo, J.F. Santa, A.Toro. Correlations between wear mechanisms and rail grinding operations in a commercial railroad. The 40th Leeds-Lyon Symposium on Tribology and Tribochemistry Forum (2013).
- [12] K. Chiddick, D. T. Eadie. Wheel / rail friction management solutions. Conference paper presented at 14th Int. Conference on Current Problems in Rail Vehicles, PRORAIL 99, Prague (1999).
- [13] J.F Santa, D. Zapata, A. Toro. Effect of rail grinding conditions on sub-surface microstructure and surface roughness of fatigued rails. First international Tribology conference. *TriBoBr* (2010).
- [14] Z. Li. Wheel-Rail Contact and Its Application to Wear Simulation. Doctoral Thesis proposal, Delft university of Technology, (2002). ISBN 90-407-2281-1.
- [15] R. Enblom. On simulation of uniform wear and profile evolution in the wheel-rail contact, Doctoral Thesis KTH, Stockholm, Sweden (2006).
- [16] R. Roberti, S. Bruni. Development of operations of tilting train on Italian network, Proceedings 5th World Congress on Railway Research, Koln, Germany, 25-29, (2001).



- [17] A. H. Wickens. Fundamentals of Rail Vehicle Dynamics, Swets and Zeitlinger, Lisse, the Netherlands (2003).
- [18] F. Braghin, S. Bruni, R. Lewis. Railway wheel wear, Wheel-rail interface handbook, (2009).
- [19] D. F. Socie, and G. B. Marquis. Multiaxial Fatigue, Society of Automotive Engineers, Warrendale, PA, USA (2000).
- [20] International Heavy Haul Association. Guidelines to best practices for heavy haul railway operations: wheel and rail interface issues. First edition (2001).
- [21] A. P. De Man. Dynatrack a survey of dynamic railway track properties and their quality. Doctoral thesis, Faculty of Civil Engineering, Delft University of Technology, The Netherlands (2002).
- [22] M. Molodova. Detection of early squats by axle box acceleration, Doctoral thesis, Faculty of Civil Engineering, Delft University of Technology, The Netherlands (2013).
- [23] Z. Li, R. Dollevoet, M. Molodova and X. Zhao. Squat growth some observations and the validation of numerical predictions. *Wear*, vol. 271, no. 1-2, pp. 148-157, (2011).
- [24] Q.Y. Liu, Z. Zhang, R. Zhou. An experimental study of rail corrugation. *Wear* 255 (2003).
- [25] T. M. Beagley. Severe Wear of Rolling Sliding Contacts, *Wear*, 36, 317-35 (1976).
- [26] P. J. Bolton, P. Clayton and I. J. McEwen. Wear of rail and type steels under rolling/sliding conditions, *ASLE Transactions*, 25, 17-24 (1982).
- [27] P. J. Bolton and P. Clayton. Rolling-sliding wear damage in rail and tire steels. *Wear*, 93, 145-65 (1984).
- [28] R. Lewis and R. S. Dwyer-Joyce. Wear mechanisms and transitions in railway wheel steels, *Proceedings I of the MechE, Part J: Journal of Engineering Tribology*, 218, 467-78 (2004).
- [29] F. Braghin, R. Lewis, R.S. Dwyer-Joyce and S. Bruni. A mathematical model to predict railway wheel profile evolution due to wear. *Wear* 261 1253–1264 (2006).
- [30] E. A. Gallardo. Temperature in a twin-disc Wheel/rail contact simulation. *Tribology International* 39 1653–166 (2006).
- [31] C. G. Saunders. Thermal Stress Relief and Associated Metallurgical Phenomena, in *Weld. Inst. Res. Bull. Vol 9 (No. 7), Part 3* (1968).
- [32] J. F. Archard. Wear theory and mechanism, in *ASME wear control handbook*, ed. By, American society of mechanical engineers, New York, 35-80 (1980).
- [33] E. Rabinowicz. *Friction and wear of materials*, John wiley and sons, New York (1965).
- [34] N. P. Suh, S. Jahanmir, E. P. Abrahamson and A. P. L. Turner. Further investigation of delamination theory of wear. *J of Lubrication Technology*, October, 631-637 (1974).
- [35] R. H. Fries and C. G. Davila. Analytical methods for wheel and Rail wear prediction, proceedings of 10th IAVSD symposium, Swets and Zeitlinger, 112-125 (1988).
- [36] P. Clayton. Tribological aspects of wheel-rail contact: a review of recent experimental research, *Wear* 191, 170-183 (1996).
- [37] M. Broster, C. Pritchard and D. A. Smith. Wheel-rail adhesion: it's relation to rail contamination on British Railways, *Wear*, 29, 309-21 (1974).



- [38] J. A. Elkins, B. M. Eickhoff. Advances in nonlinear Wheel/rail force prediction methods and their validation ASME winter annual meeting, New York, USA (1979).
- [39] Z. Li, J. J. Kalker. Adaptive solution of rolling contact using boundary element method, Proc. the 20th World conference on the boundary element, 19-21 August, Orlando, Florida, USA (1998).
- [40] H. Hertz. Ü ber die Berührung zweier, fester elastischer Körper, Journal für reine und angewandte Mathematik, 92, 156–171 (1882).
- [41] K. L. Johnson. The strength of surfaces in rolling contact, Proceedings Institution of Mechanical Engineers, 203, 151-63 (1989).
- [42] R. Lewis and U. Olofsson. Mapping rail wear regimes and transitions, Wear, 257 721-9 (2004).
- [43] J. Ayasse, H. Chollet. Wheel-Rail contact. Handbook of Railway Vehicle Dynamics, chapter 4, 2006.
- [44] F. W. Carter. On the action of a locomotive driving wheel. Proc. Royal Society, London, A 112 (1926).
- [45] R. Enblom. On simulation of Uniform wear and profile evolution in the wheel-rail contact. Doctoral Thesis in railway technology, Royal institute of Technology, OLD ISB 91-7178-605-1. Stockholm (2006).
- [46] J. J. Kalker. On the rolling contact of the Elastic Bodies in the presence of dry Friction. Doctoral Thesis, Delft (1967).
- [47] J. J. Kalker. Rolling contact phenomena – linear elasticity. In: CISM international center for mechanical sciences, Vol 411. Springer, New York, 2001, ISBN: 3-211-83332-3 (2001).
- [48] N. Burgelman, Z. Li, R. Dollevoet. A new rolling contact method applied to conformal contact and the train-turnout interaction. Wear 2014.
- [49] O. Polach. A fast wheel-rail forces calculation computer code. ADtranz, Winterthur, Switzerland (2000).
- [50] Isao Okamoto. How bogies works. Railway technology today 5, Pag 52-61. (1998).
- [51] A. R. Martinez. Rediseño de un dispositivo elastomérico de suspensión ferroviaria para mejorar el desempeño de un vehículo de pasajeros de un sistema metro. Master thesis, Eafit University. (2010).
- [52] O. Polach, M. Berg, and S. Iwnicki. Simulation, Handbook of Railway Vehicle Dynamics, chapter 12, 2006.
- [53] T. Jendel. Prediction of wheel profile wear—comparisons with field measurements. Wear 253 89–99 (2002).
- [54] M. Ignesti, M. Malvezzi, L. Marini, E. Meli, A. Rindi. Development of a wear model for the prediction of wheel and rail profile evolution in railway systems. Wear 284-284 (2012).
- [55] Y.Q. Sun, C. Cole, P. Boyd. A numerical method using VAMPIRE modelling for prediction of turnout curve wheel–rail wear. Wear 271 482–491 (2011).
- [56] J. Kalousec and E. Magel. Modifying and Managing Friction. Railway and Track Structures (1999).



- [57] L. J. Wilson. Performance measurements of rail curve lubricants. PhD. thesis. Queensland University of Technology, Australia. 2006
- [58] Y.A. Areiza. Efecto de la fuerza de fricción en el contacto rueda-riel sobre el consumo medio de energía en operación del metro de Medellín. Master thesis, National University of Colombia. (2014).
- [59] L. Castañeda, J. Gallego, R. Martinod. Dynamic analysis to evaluate stability, safety and comfort in railway vehicles. 23rd ISPE International Conference on CAD/CAM Robotics and Factories of the Future (2010).
- [60] R. Martinod, G. Betancur, L. Castañeda. Identification of the technical state of suspension elements un railway systems. Vehicle System Dynamics (2012).
- [61] S. D. Iwnicki. Handbook of Railway Vehicle Dynamics. Taylor and Francis Group, Boca Raton, Florida (2006).



**NATIONAL UNIVERSITY OF COLOMBIA
FACULTY OF MINES
SCHOOL OF MINERALS AND MATERIALS
MEDELLÍN
2015**